Design and Evaluation of a Soft Hydro-Pneumatic Haptic Ring for Multimodal Texture Rendering

Ana Sanz Cozcolluela

Delft University of Technology

TU Delft

Design and Evaluation of a Soft Hydro-Pneumatic Haptic Ring for Multimodal Texture Rendering

by

Ana Sanz Cozcolluela

to obtain the degree of
Master of Science in Mechnical Engineering
at the Delft University of Technology,
to be defended publicly on Friday September 6, 2024

Student number:	5827094
Supervisor:	Dr. Y. Vardar
Project Duration:	November, 2023 - September, 2024
Thesis Committee:	Dr. Y. Vardar, TU Delft, Chair
	Dr. B. Fereidoonnezhad, TU Delft, External member
	Dr. S. Ghodrat, TU Delft, External member
	Dr. J. Jovanova, TU Delft, External member

TU Delft

Acknowledgements

This thesis is dedicated to everyone who has supported and inspired me throughout my academic journey, to those who have helped me grow as a student, as a researcher, and as a person.

To my supervisor, Yasemin Vardar, for giving me the chance of working on such an innovative project. Thank you for your support, guidance and dedication. Your passion and enthusiasm have truly been inspiring.

To my fellow HITLab members, thank you for your assistance and for every enriching discussion we had. You made every challenge and every break a lot more fun.

To all my friends, for staying by my side and for always listening to my problems, frustrations and triumphs. To my family, to those who are here and those who are gone, and especially to my parents, thank you for your unconditional support and love.

To the Euros and the Olympic Games, for making the last months of my thesis much more entertaining. And lastly, I would like to thank myself. Quoting Ursula Corberó's words ”Me lo dedico a mi, por ser tan trabajadora y tan valiente, porque estuve a esto de decir que no a este personaje, y por ser tan maja” [1].

Ana Sanz Cozcolluela
Delft, August 2024

[1]”I would like to thank myself, for being so hardworking and brave, because I was on the verge of saying no to this character, and for being so nice.”

Contents

1

Paper: Design and Evaluation of a Soft Hydro-Pneumatic Haptic Ring for Multimodal Texture Rendering

Design and Evaluation of a Soft Hydro-Pneumatic Haptic Ring for Multimodal Texture Rendering

Ana Sanz Cozcolluela

***Abstract*—With the growing popularity of virtual and augmented reality, there is an increasing demand for haptic devices that can replicate naturally occurring tactile sensations. Specifically, multimodal devices capable of delivering multiple types of haptic feedback simultaneously are crucial for enhancing realism and immersion. In this paper, we introduce a novel, entirely soft, multimodal haptic ring designed to provide vibratory, pressure, and thermal stimuli. Our ring, targeted for texture rendering applications, integrates pneumatic and hydraulic circuits to accurately simulate the roughness, temperature, and compliance cues experienced when freely exploring surfaces with the fingertip. We validated the performance of our system through a psychophysical experiment, which demonstrated that participants could match virtual textures displayed by the ring with real textures with up to 90 % accuracy for several surfaces. Participant's adjectives ratings indicated that the ring can provide distinctly different stimuli in all of the rendered perceptual dimensions, closely matching those of real textures. This study shows that by relocating tactile feedback from the fingertip, our ring offers maximum wearability, enabling free exploration of surrounding environments and full range of motion, highlighting its potential in mixed reality applications.**

***Index Terms*—Haptics, wearable, multimodal, soft actuator, pneumatic, hydraulic, texture rendering**

I. Introduction

THE sense of touch plays a crucial role in our everyday lives, serving as the main mean through which we interact with our surrounding environment. Without it, simple tasks such as grabbing an object or pushing a button become increasingly challenging. As such, there is a growing interest in simulating the sense of touch, particularly in scenarios where tactile information is limited, such as robot teleoperation, medical devices or the automotive industry [1].

Haptic devices, which aim to simulate naturally occurring tactile cues though the use of mechatronic components, are gaining increasing relevance [2]. It is of special interest their application to virtual reality (VR) and augmented reality (AR), particularly in the form of wearable haptic systems. These untethered devices, worn around the body, interact directly with the skin, offering the potential for comfortable and realistic interactions while permitting natural body movements.

Despite their growing popularity, most wearable haptic devices still present shortcomings in terms of their weight, flexibility and ease of wear. Many incorporate rigid and bulky materials which conflict with the flexible nature of the human body and hinder natural sensations and interactions [3]. Additionally, many existing systems face significant limitations in terms of realism and simulation quality, as they typically rely on a single type of haptic feedback. Given that when we explore our surrounding environment we perceive multiple sensations at once, such as surface temperature, roughness or softness, providing one single type of cue is insufficient. Although there are a number of haptic devices that provide multiple stimuli simultaneously, they are often tool-based and make use of pen-like designs [4], [5] not appropriate for VR applications, where being limited to a screen highly decreases immersion.

To address these limitations, soft robotics has emerged as an exciting media for developing lightweight, wearable and flexible interfaces specifically designed to be compatible with the human body without causing discomfort or distraction [6]. Affordable and generally easy to design and produce, these soft interfaces could incorporate multiple actuation and feedback mechanisms within one system, enabling the delivery of realistic haptic interactions.

In this study, we propose a soft multimodal ring capable of independently providing vibrotactile, pressure and thermal cues. Our system integrates a hydraulic circuit to deliver thermal stimuli with a pneumatic system that provides pressure and vibrotactile cues. The ring, made entirely out of silicone, is lightweight and comfortable, offering maximum adaptation to the skin. Worn around the phalanx, it relocates stimuli away from the fingertip, allowing for full hand motion and unrestricted environment exploration. Designed for multimodal texture rendering in virtual reality, our ring simulates the interactions occurring when touching surfaces with the fingertip, mimicking real textures with high fidelity in their roughness, thermal and compliance dimensions.

This paper is structured as follows. Section II provides an overview of the state of the art on soft haptic hand-worn systems. Section III focuses on device concept and design, describing its fabrication process and components used to drive the system. Section IV illustrates the rendering approaches selected to simulate roughness, compliance and thermal stimuli, followed by Section V, which illustrates the methodology for the psycophysical experiment, including the texture selection and validation process. The results of the study are presented and discussed in Section VI and VII, respectively. Finally, conclusions are detailed in Section VIII.

II. State of the art

The hands are among the most sensitive areas of the body and serve as the primary medium for interacting with the environment. Consequently, it is unsurprising that most wearable haptic devices are designed to be worn on the hands. While many of these devices focus on providing kinesthetic

feedback and simulate the forces and motions involved in interacting with and grabbing objects [7], there is a growing interest in devices that deliver tactile feedback, simulating surface-level cues such as pressure, vibration, or temperature [8].

Most tactile feedback devices adopt glove-like designs, which, despite their intuitive interfaces, often suffer from being cumbersome, heavy, and restrictive. These gloves can impede hand movements and since they typically cover the fingertips, pose challenges for finger tracking and natural interaction with the environment. This is particularly problematic in mixed and augmented reality applications, where users may need to interact with both real and virtual environments. To address these issues, ring interfaces offer a solution by relocating stimuli from the fingertip to other areas of the finger [9].

A variety of haptic rings have been developed by multiple research groups. For example, Pacchierotti et al. [10], designed the h-Ring, which employs two servo motors to move a belt that presses into the user's proximal phalanx, applying shear forces and simulating contact with objects. Similarly, Gaudeni et al. [9] designed a vibrotactile ring based on a voice coil actuator and showed that the proximal phalanx is the most promising location for vibrotactile relocation. Nevertheless, these devices, as well as most currently available haptic rings, only present one feedback modality, which highly reduces the variety of haptic effects that can be delivered. A promising approach to overcome this limitation is the development of multimodal haptic systems that integrate multiple modalities within a single device.

Although less common than their single-mode counterparts, there are several examples of multimodal haptic rings. For instance, van Riessen et al. [11] developed a ring that provides thermal cues at adjustable contact pressures by integrating a thermoelectric module with a servo motor-driven belt. Similarly, Sun et al. [12] designed a ring capable of delivering both vibration and thermal cues using small vibration motors and nichrome heaters. These devices however, are limited by their rigid character, as they incorporate rigid and bulky components that can be uncomfortable for the user. To address this issue, soft haptic interfaces offer a promising alternative, as they can better conform to the skin and provide more realistic and comfortable haptic experiences.

There is a growing number of soft haptic devices, particularly pneumatic-based ones, mainly due to their fast response times, low-cost components and large deformations with high power-to-weight ratios. One of the most relevant examples is the soft multimodal ring proposed by Talhan et al. [13], which is able to deliver static pressure, high-frequency vibration, and impact force feedback by inflating a pneumatic ring at different patterns. Although pneumatic systems are among the most popular, a number of devices employ other types of actuation, often based on hydraulics. These systems present similar characteristics to pneumatic systems yet show improved drive efficiency and dynamic behaviour. Additionally, as presented by Han et al. [14], hydraulic systems can be employed to provide not only pressure or vibration cues but also thermal feedback by pulsing water at different temperatures through a display.

Despite the multimodal character of these devices, many still rely on a single actuation approach, which often means that only one type of cue can be delivered at a time. Hashem et al. [15] addressed this limitation by incorporating a dual-layer air chamber into their wearable thimble, enabling the simultaneous delivery of vibration and pressure feedback by independently actuating each chamber, which proved to significantly improve realism. Another potential solution is to integrate different types of actuation within a single device. Although this approach is less common and has not been widely applied in ring interfaces, there are examples of soft wristbands that combine pneumatic and thermal actuation [16], or hydraulic and thermal actuation [17], primarily for social touch applications. These devices have demonstrated that incorporating temperature cues can enhance the overall pleasantness and comfort of the experience.

Additionally, a significant limitation of most soft haptic devices is that they generally only provide simple haptic patterns such as discrete forces, temperatures or vibrations. Very few works are targeted for texture rendering, with Talhan's [18] multimodal haptic thimble and Hashem's dual chamber thimble [15] being some of the only examples. Even these devices have limited texture rendering capabilities, primarily simulating roughness through vibration cues while neglecting other dimensions like softness, temperature, or friction. Moreover, the textural patterns they provide are simplified and not based on data from natural unrestricted surface exploration with the finger.

This work addresses these limitations by developing a soft haptic ring that relocates stimuli from the fingertip. By incorporating two distinct actuation mechanisms, we created a multimodal device capable of delivering pressure, vibration, and temperature cues. The design focuses on texture rendering, achieved by simulating finger interactions with real surfaces. To the best of our knowledge, our system is the first of its kind, being the only soft ring incorporating multiple actuation mechanisms and three haptic feedback modalities within a single interface. Additionally, its focus on multimodal texture rendering using finger texture exploration data, makes our device unique in the field.

III. Device concept and design

A. Device concept

The focus of this work is to design a haptic system capable of rendering textures for virtual reality applications. Our goal is to address the limitations of existing systems, which are often rigid, bulky, and provide only simple haptic patterns while obstructing the fingertip. Therefore, our system must satisfy the following requirements:

- Flexible, lightweight, and compact design.
- Unobstructed fingertip to allow natural interactions.
- Multimodal device capable of generating pressure, vibration, and thermal cues.

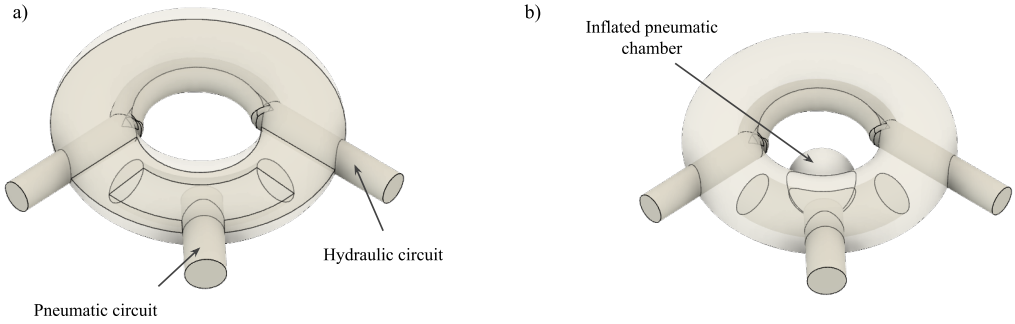

Fig. 1: Ring design concept in its inactive state (a) and in its inflated state (b)

- Independent and simultaneous delivery of haptic stimuli.

The first and second requirements are addressed by selecting a completely soft ring as our haptic interface. A ring worn on the phalanx ensures that the fingertip remains unobstructed, allowing for natural hand movements and unrestricted environment exploration. Similarly, by manufacturing the ring out of silicone, flexibility, lightweightness and compactness can be maximized while allowing for easy production of various sizes that accommodate different finger sizes.

The third requirement is more challenging to complete in a soft interface, particularly the integration of thermal feedback into the system. Typically, thermal stimuli are generated using thermoelectric devices [19], however, their rigid character would compromise the flexibility of our soft ring. Similarly, while piezoelectric actuators can deliver complex vibration patterns [20], their incorporation could impact negatively toward the ring's soft character. To overcome these challenges, we settled for a design combining a hydraulic and a pneumatic system. The hydraulic circuit pumps water at varying temperatures through the ring, providing thermal stimuli. Meanwhile, the pneumatic system is used to inflate a chamber within the ring, delivering vibratory cues through the rapid inflation and deflation of the pocket. Similarly, pressure stimuli can be provided by adjusting the inflation patterns of the chamber. By incorporating these two actuation approaches, the fourth requirement is also satisfied, as both systems operate independently and can generate stimuli simultaneously.

At initial stages of the design process, we considered implementing a hydraulic-only system to simplify ring design and reduce components. However, we soon realized that the higher response times of water compared to air would prevent the rendering of complex haptic pressure and vibration patterns. Additionally, it could present issues related to unwanted oscillations, unreliable inflation due to air bubbles and greater bursting and failure potential. Because of this, including a pneumatic system was seen as the most suitable solution despite increasing device complexity.

From a design perspective, as illustrated in Figure 1, our haptic interface features a pneumatic chamber on the front of the ring, which will be in contact with the ventral phalanx. This location, on the same side as the fingertip, should simulate realistically the feeling of touching a surface while offering high sensitivity [21], [22]. On the dorsal side of the ring, in contact with the back of the phalanx, there is a space housing a thin silicone tube part of the hydraulic circuit. This tube channels water at various temperatures to provide thermal cues, exploiting the higher thermal sensitivity of the hand dorsum, especially for cold stimuli [23]. As seen, rather than designing an embedded hydraulic chamber similar to the pneumatic one, a silicone tube was inserted on the ring itself. Initial trials revealed that the manufactured silicone ring exhibited very low thermal conduction, even when designing thin walls, which also led to their possible bursting at high pressures. Using a silicone tube instead allowed us to overcome these challenges and prevent nicking, leakage or vibration issues.

Our ring design implies that pneumatic and thermal cues are provided in opposite locations of the finger, which was a deliberate choice to increase comfort by ensuring that the hydraulic tube would not displace even when high vibratory or pressure stimuli are provided. However, this design may create a sense of incongruity, as stimuli are perceived at multiple locations rather than at a single localized spot as it occurs in natural tactile exploration. Despite this discrepancy and given that human localization of thermal stimuli is poor [24], we expect that by actuating both thermal and pressure systems simultaneously, we will be able to elicit a tactile illusion of thermal referral [25]. This principle states that when temperature and tactile sensations are given to two nearby points on the skin, temperature is also perceived where the tactile sensation is given. Using this phenomenon, we aim to generate stimuli more closely reassembling those naturally perceived at the fingertips.

B. Ring fabrication

To fabricate our soft ring, EcoFlex 00-30 is used as the main material. With a low elastic modulus between 100 and 125 kPa, its stiffness is within the range of human skin. This behaviour in combination with its soft, strong, and stretchy character, sets silicones as ideal materials for wearable and skin-attachable devices [26].

The ring manufacturing process involves several steps, as depicted in Figure 2. First, we 3D-print two identical plastic molds to create two halves of the ring. These molds, made from polylactic acid (PLA), are designed to split the ring along its transversal plane and are further divided into two parts for easier demolding. To accommodate for various finger sizes, three different molds with an internal diameter of 15, 18.5 and 22 mm, are available. Special care was taken when designing the molds to guarantee that the volume of the pneumatic chamber is kept constant, ensuring that all rings have similar inflation characteristics despite their different size. Technical drawings of the molds can be found in the Appendix.

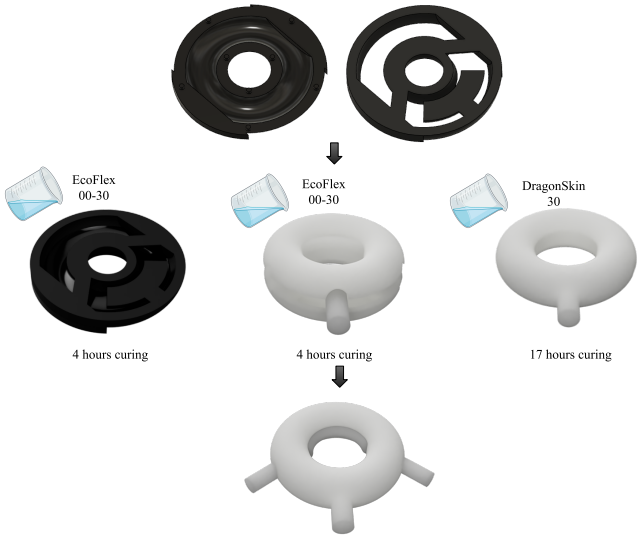

Fig. 2: Ring manufacturing process including mold design, casting and tube insertion

The subsequent step involves casting the molds, which begins by mixing part A and part B of the EcoFlex silicone rubber in equal parts. After throughout stirring and lining of the molds with release agent for better demolding, the mix is poured into the molds and left to cure for at least four hours at room temperature. Afterwards, the two halves are joined together using the same silicone mix. During this step, a thin 4 mm diameter silicone tube, which will later enable the inflation of the pneumatic chamber, is inserted between both halves. As such, the accurate alignment of all elements is essential to obtain a robust product.

The insertion of the tube with the ring is, despite perfect alignment, the weakest point of the design, as it is the area where the ring may burst the most easily at high pressures. To avoid this issue, the insertion is lined with Teflon tape, covered with a Ecoflex 00-50 layer and finally left to cure for seventeen hours. The higher Young's modulus and stiffer behaviour of this silicone mix combined with the thin Teflon tape layer ensures that the tube remains in place and does not leak or burst at high pressures. During this process, it is of importance to only pour the new silicone mix at the tube insertion and put particular care into not covering the inner part of the ring so that the actuator's inflation characteristics remain unchanged.

During the final step of the manufacturing process, a strain limiting fabric layer is applied to the upper, lower and outer surfaces of the ring using Sil-Poxy silicone adhesive. This process ensures that when filled with air, only the inner surface of the ring will inflate and provide localized pressures at the frontal side of the phalanx. Additionally, during this step, a thin 2 mm silicone tube connecting to the hydraulic circuit to present thermal cues to the dorsal side of the phalanx, is embedded on the inner surface of the ring. Figure 3 shows the final result of the manufacturing process.

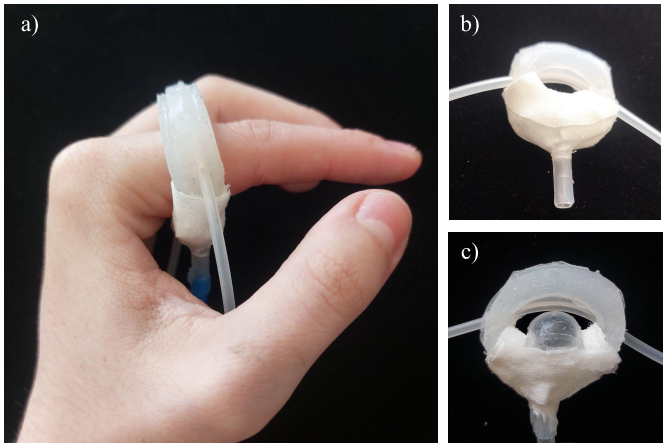

Fig. 3: Ring final product worn by user (a), ring when deflated (b) and ring with inflated pnuematic chamber (c)

C. Hydraulic circuit

To provide thermal cues, the haptic ring makes use of a hydraulic circuit, as illustrated in Figure 4, which pumps water through the silicone tube at different temperatures. The circuit is composed of a hot tank and a cold tank whose water is combined in a mixing container and then pumped to the ring. The hot water tank maintains a constant temperature of 42.5 °C, regulated by a 300 W submersible heating element (860-6921, RS PRO). The cold water tank is kept below 5 °C by continuously adding ice. Water from these containers is sent to the mixing tank using two independent water pumps (KW-1646, Kiwi Electronics). From the mixing tank, water is pumped through the silicone tube embedded in the ring using a third water pump. After circulating through the ring, water returns to the mixing tank, completing the cycle.

Although the addition of a mixing water tank rather than pumping water to the ring directly may lead to slower times in reaching the required temperatures, it ensures a more uniform water mixing that enables a more stable temperature control. To mitigate delays due to the mixing tank, its water level is maintained at a minimum by a non-contact liquid level sensor (XKC-Y25-NPN) and a hydraulic pump that sends water back to the hot and cold tanks. To prevent water backflow and unintended mixing between the tanks, a solenoid valve (ADA-997, Adafruit) is employed. Additionally, a smaller

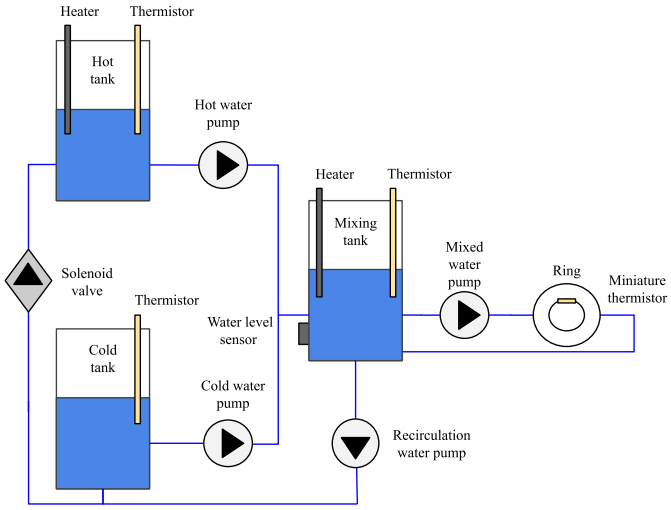

Fig. 4: Schematic of the hydraulic circuit

100 W submersible heating element (860-7163, RS PRO) in the mixing tank further reduces waiting times by activating when the water temperature falls below a set value.

Water temperature in the hot, cold and mixing tanks is constantly monitored by submersible NTC thermistors (B57861S0103F040, EPCOS). To accurately control the temperature experienced by the user, a miniature NTC thermistor (GA10K3MBD1, TE Connectivity) is placed between the silicone tube and the ring, measuring the external temperature of the hydraulic tube.

D. Pneumatic circuit

In order to render vibration and pressure cues, a pneumatic circuit connected to the ring's pneumatic chamber, as seen in Figure 5, is employed. This circuit includes two different sections connected in parallel to generate pressure and vibration stimuli, respectively.

The main component used to produce vibration cues is a fast-switching three-way solenoid pneumatic valve (MHE2-MS1H-3/2G-M7, Festo), chosen due to its high switching frequency of 300 Hz. This valve is supplied at its inlet port by an air compressor (FD-186, Fengda) whose pressure is monitored and kept at a constant value of 75 kPa by a mechanical pressure regulator (AR-200, LNCN) and a digital pressure gauge. This pressure provides sufficient and perceivable inflation of the ring actuator while preventing excessive blowing that may lead to its bursting. The valve's output port is connected in parallel through a 1:2 Y-connector to the ring, while the remaining port of the valve, the exhaust, is outfitted with a silencer that reduces noise. This configuration allows air to flow freely and inflate the ring when the valve is at its active state, while when inactive, air is blocked at the inlet port of the valve. In this way, when inactive, the ring is connected to the exhaust port, allowing air to escape out of the circuit and deflate the actuator. Consequently, the quick activation and deactivation of the fast-switching solenoid valve leads to the rapid inflation and deflation of the ring, providing vibrating cues.

Although this valve could also be employed to provide pressure cues by controlling its switching times, inflating the pneumatic chamber in a controllable manner using this approach proved challenging. Additionally, this configuration does not allow air to be maintained inside the ring or for it to be expelled at varying speeds, instead, the actuator can only inflate continuously or deflate sharply. This poses a challenge for our application, in which we may want to inflate the actuator at different speeds to simulate materials with different stiffnesses, or maintain air inside the actuator for prolonged periods of time to provide the illusion of keeping contact with a surface. To solve these issues, an additional pressure rendering system is connected in parallel to the vibration valve through the previously mentioned Y-connector.

This pressure rendering system simply consists of a linear actuator that pushes and pulls a syringe connected to the ring. By adjusting the speed of the linear actuator, the ring can exhibit various inflation profiles. Additionally, when the linear actuator and the vibration valve are not in operation, air should remain trapped in the closed circuit between the syringe and the ring to keep the actuator inflated. However, due to the low pressures employed to operate our circuit, the fast-switching solenoid valve exhibits small leakage at its close state, preventing the ring from staying inflated. This issue was resolved by adding an additional normally closed two-way solenoid pneumatic valve (MHA1-M1H-2/2G-0,9-PI, Festo) in between the vibration valve and the Y-connector. In this way, to provide vibratory stimuli, the valve remains at its open state, allowing air to flow to the ring. Conversely, when providing pressure stimuli, the valve closes, enabling the ring to inflate, maintain its inflation, or deflate, based on the operation of the linear actuator controlling the syringe.

As a result, the designed pneumatic circuit can deliver both vibratory and pressure stimuli, as illustrated in the Appendix. However, these stimuli cannot be provided independently. As seen, the actuator can not inflate when the ring is vibrating, and vice versa. This limitation could be addressed by adding an extra pneumatic chamber to the ring, with one chamber dedicated to vibration and the other to compliance. Nevertheless, given that such an addition would increase ring size and design complexity, we chose to proceed with our single-chamber design.

E. System control

The complete system is fully controlled by an Arduino Mega microcontroller. All the hydraulic pumps as well as the linear actuator and pneumatic valves are enabled by dual H-bridge motor drivers (L298N, Kiwi Electronics), which allow the independent power control of every element. In contrast, each of the heating elements is regulated by a relay module, enabling their safe and independent toggling.

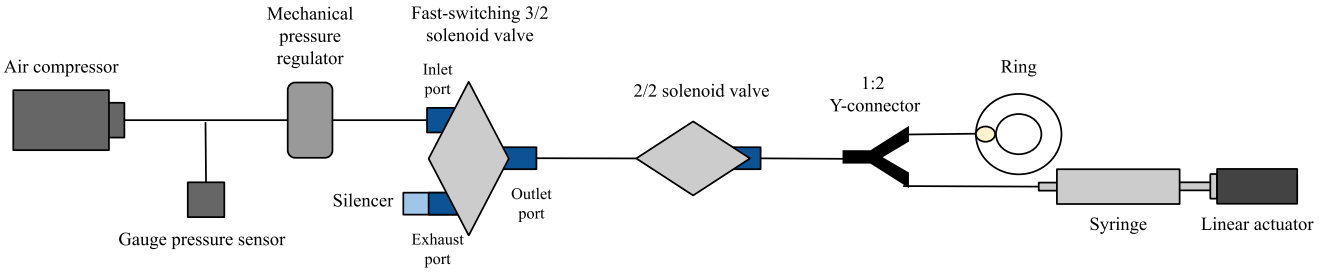

Fig. 5: Schematic of the pneumatic circuit

While the pneumatic components of the circuit are controlled by directly toggling their activation states, the hydraulic elements require a more complex control algorithm. Specifically, the pumps directing water from the hot and cold tanks to the mixing tank are regulated by a proportional controller which dynamically controls pump speed according to the difference between the target display temperature and its actual value, as seen in Equation 1,

$$r(t) = K_p \cdot e(t) = K_p \cdot (T_t - T_c) \tag{1}$$

where the proportional gain K_p equals 17.5 and T_t and T_c represent the target and current display temperatures, respectively, both normalized to a temperature range between 45 and 10°C. As explained by Choi et al. [27], the sign of the output signal $r(t)$ denotes whether heating or cooling is required, which after being normalized to the -1.0 to 1.0 range, is used to compute the PWM parameter that drives the hot or cold pump. In this way, as the error decreases, both $e(t)$ and $r(t)$ should converge to zero, leading to the progressive decrease of the PWM parameters. The proportional gain K_p was attentively tuned, and after careful consideration, we chose not to implement derivative or integral control. This decision is based on the inherently slow response of water, which needs to heat up and cool down to change the temperature of the silicone tube used as display, also exhibiting slow heat conduction. Given this behavior, adding integral or derivative terms did not significantly improve performance, so we opted for the simpler yet effective proportional controller.

As seen, one of the main limitations of our hydraulic circuit and its controller is that it employs the external temperature of the display as the control variable. This behaviour allows for a more accurate control of the displayed thermal stimuli, however, it also implies that water has to be circulating constantly through the tube to be measured by the temperature sensor. As a consequence, the user will feel temperature stimuli before the actual thermal simulation begins, which may be seen as confusing or counter-intuitive, especially at initial stages.

IV. Texture rendering

A. Texture database

One of the key novelties of our system is its application in multimodal texture rendering, mainly intended for its use in virtual or mixed reality scenarios. Our goal is to generate realistic cues that mimic the sensation of exploring surfaces, for which it is crucial to use data that captures the interaction between bare fingers and real surfaces. For this purpose, we utilized the SENS3 database by Balasubramanian et al. [28], including physical interaction data recorded as participants explored fifty different surfaces with their bare fingers using four distinct exploratory procedures: static contact, pressing, tapping, and sliding.

The database provides information about thermal interactions recorded during static contact exploration, including skin temperature and heat flux between the skin and the surface. During the pressing procedure, force-indentation depth data was collected to analyze how different textures respond to finger pressure. Surface hardness was captured by recording acceleration during the tapping procedure, while friction and roughness were documented by measuring finger acceleration and forces during the sliding procedure. Additionally, the database includes top-view high-resolution surface images for each texture and auditory data corresponding to the sounds produced during surface interaction. Perceptual data, in the form of adjective ratings that describe the psychophysical sensations experienced while exploring different surfaces, are also included.

The SENS3 database is one of the few resources that records bare-finger interactions and incorporates not only acceleration and force data but also thermal, visual, and adjective rating information. Consequently, we chose to use this dataset to render the textures that will be displayed by our soft haptic ring.

B. Temperature rendering

Providing temperature cues that simulate the thermal characteristics of a material and thus the heat transfer between the skin and a surface is not a straightforward process. Most models that aim to describe this interaction are based on bio-heat equations [29] and do not take into account the thermal contact resistance that arises between the skin and an object.

To avoid this limitation, the semi-infinite body model taking into consideration the influence of thermal contact resistance by Ho and Jones [30], [31], can be employed.

This model considers that the thermal interaction between the skin and a material with which it is in contact is a transient process dominated by heat conduction. In this process, heat is transferred across the interface and flows through a thermal contact resistance. Consequently, during contact, the heat flux of the skin and that of the material will be identical, where the flux is determined by the difference between the skin surface temperature and the object surface temperature divided by the thermal contact resistance. This relationship is described by Equations 2 and 3, where $q''_{skin,s}$, $q''_{object,s}$, $T_{skin,s}$ and $T_{skin,s}$ refer to the heat flux and temperature of the skin and object surfaces, respectively, and $R_{skin,object}$ stands for the thermal contact resistance between skin and object.

$$q''_{skin,s} = q''_{object,s} = q'' \tag{2}$$

$$q'' = \frac{T_{skin,s}(t) - T_{object,s}(t)}{R_{skin,object}} \tag{3}$$

Thermal contact resistance itself depends on a number of variables related to the thermal and mechanical properties of the contacting surfaces. For materials with an even surface and interaction contact forces around 2 N, it can be approximated by Equation 4, where k_{object} is the thermal conductivity of the object.

$$R_{skin,object} = \frac{0.37 + k_{object}}{1870 \cdot k_{object}} \quad [m^2K/W] \tag{4}$$

The semi-infinite body model can be further extended to predict the temperature at which a thermal display should be activated to reproduce the thermal characteristics of an object in contact with the skin [32]. This can be done simply by replacing the object terms of the previous equations with those of the display:

$$q'' = \frac{T_{skin,s}(t) - T_{object,s}(t)}{R_{skin,object}} = \frac{T_{skin,s}(t) - T_{display}(t)}{R_{skin-display}} \tag{5}$$

$$T_{display}(t) = T_{skin,s}(t) \cdot [1 - \frac{R_{skin,display}}{R_{skin,object}}] + \frac{R_{skin,display}}{R_{skin,object}} \cdot T_{object,s}(t) \tag{6}$$

These equations, when combined with Equation 3, yield an expression that allows us to compute $T_{display}$ as a function of the heat flux and the thermal contact resistance between the skin and thermal display:

$$T_{display}(t) = T_{skin,s}(t) - q'' \cdot R_{skin-display} \tag{7}$$

Hence, to simulate object-skin interaction temperatures with a thermal display, it is necessary to know the skin temperature when in contact with the object, as well as the heat flux and the thermal contact resistance between the skin and the display. The later, for the designed display, which is simply the silicone tube embedded in the ring, can be estimated to be 0.0015 m^2K/W [33]. In contrast, the skin temperature and heat flux, due to their dynamic character, cannot be estimated easily and require real interaction data. For this purpose, we employed the thermal recordings collected at the SENS3 database.

As such, we first process the skin temperature and heat flux data by using a 10 Hz and a 1 Hz low-pass filter, respectively, to remove high frequency noise. Following this step, we discard the first elements of the data in which the finger is not yet making contact with the surface, as the employed model is only valid during skin-object contact. These computations allow us to determine the display temperature as a function of time, which can directly be used by our control algorithm. However, in order to reduce data length and complexity, we first fit a seventh order polynomial through the display temperature curve. This fitted curve is then sent to the microcontroller, which actuates the hydraulic circuit and pumps water through the tube to display the required thermal profiles. These steps are shown with greater detail in the Appendix.

C. Roughness rendering

Most haptic devices rendering roughness use vibrotactile actuators to simulate the surface characteristics of textures by generating vibrating stimuli. These systems typically rely on algorithms that employ force or acceleration signals obtained when sliding a pen-like tool against a surface [34]. These signals are then processed and modulated to determine the actuation frequencies and amplitudes [35], [36].

Initially, we tried applying this approach to the SENS3 database's sliding data. Since the data were recorded at varying forces and exploration speeds, we first isolated intervals where both the applied normal force and exploration speed were constant. We experimented with sliding force data along one axis, friction force, and sliding acceleration signals, however, none of these signals were suitable for our application, as most of the computed frequencies exceeded the maximum switching frequency of our pneumatic valve. This limitation caused the valve to act as a low-pass filter, ignoring high-frequency components and producing similar output profiles for different textures, particularly when rendering smooth or fine textures. Additionally, our results were limited by the valve's controllability, as we can only adjust its activation times, and thus control rendered frequency but not amplitude. As a result, it is imperative that the signal sent to our fast-switching solenoid valve is a binary square wave with only two states, high and low, where their timing determines the system's vibration frequency.

Given these constraints, we decided to disregard the sliding signals in favor of a simpler image-based approach. Our method involves an intensity-based algorithm combined with a peak detection function, which we applied to high-resolution surface images. This approach assumes that textures exhibit different intensities based on their surface and roughness

characteristics. As such, smoother textures generally have homogeneous intensities across their profiles, while rougher textures show greater variance due to surface features like bumps and creases.

To implement our method, we first apply a mean filter to the grey-scaled surface images to reduce noise and avoid potential high frequencies that our valve cannot reach. Next, we convert the two-dimensional image into a one-dimensional signal by selecting a single line of pixels extending throughout the entire texture's width at its middle height. This signal can then be transformed into a pulse wave suitable for our valve by applying a threshold, where values below the threshold correspond to the valve's inactive state, while values above the threshold activate the valve. Nevertheless, we soon realized that this thresholding approach may produce undesired results, as it is influenced by the absolute intensity of the texture. As such, dark yet rough textures would present low intensities and could be mistaken as smooth. To address this issue, we implemented a peak detection algorithm using MATLAB's *findpeaks* function [37] to consider the relative intensity of the signal rather than its absolute value. Using this function, we can ensure that the minimum distance between events is that of our valve's operating frequency, but more importantly, it allows us to select peaks or events based on their prominence, or height relative to other peaks. In this way, the detected local maximum or peaks indicate when the valve should be turned off, while the valleys or local minimum indicate when it should be activated. As such, the output of the algorithm is a binary square wave based on pixel location, which we then convert to a time-based signal using a conversion factor of 5 cm/s, which was seen as a suitable and dynamic exploration speed that would allow us to still respect the limitations of our valve.

Despite the advantages of our peak detection algorithm, it has limitations when handling surfaces with very high frequencies, such as fabrics or cardboard. These textures produce intensity signals with small, high-frequency peaks that our algorithm may fail to detect, rendering them as overly rough surfaces. To mitigate this problem, we manually adjusted the square wave frequencies for these very fine textures to match our valve's maximum operating frequency. This process as well as the previous steps are further explained in the Appendix.

D. Compliance rendering

By delivering pressure stimuli we aim to simulate the compliance of different materials, for which we employ pressing data from the SENS3 database. While tapping recordings could have been used for this purpose, we settled for pressing data, as they represent a slower finger motion that is simpler to simulate and easier to integrate with other rendering modalities. In this way, the pressing data employed corresponds to the force applied when slowly pressing a surface and then maintaining static contact with it.

Rendering these signals with our ring is a challenging process, as our pneumatic actuator has an inflation profile that cannot be easily changed to match real texture data. Initially, we attempted a closed-loop control strategy to simulate these curves, based on monitoring applied actuator force and regulating airflow accordingly. However, this approach proved inconsistent and unreliable due to the small force magnitudes and low air pressures involved. To address these issues, we adopted instead a simplified approach based on pressing rate to determine the actuator's inflation rate. In this way, for each signal, we identified the time at which maximum force is applied, marking the end of the pressing phase and the beginning of static contact. Using this data we computed the pressing slope for each texture and mapped them to our linear actuator speed range, allowing us to achieve different inflation rates. As such, with this approach a material with a smaller pressing slope corresponds to a softer material, which, due to its slower inflation speed, produces lower forces. Conversely, a stiffer material shows a higher inflation rate, resulting in faster and stronger forces due to its steeper pressing slope. This same procedure was then applied to determine the deflation speed by identifying the point where applied force begins to decrease, indicating the start of finger lift-off and loss of contact with the surface. Again, a softer material deflates more slowly, while a stiffer one deflates more sharply. In this case however, the differences in deflation speed among distinct materials are less pronounced.

As a result, we obtain a trapezoidal signal where the rising and falling slopes correspond to the actuator's inflation and deflation speeds, respectively. In this way, during the static contact phase of the signal, the rendering signal corresponds to a flat curve where the applied force remains constant. Although the actual pressing signals in the database show a slow decrease in force during this interval, we decided to simplify our model due to the limited controllability of our syringe-linear actuator setup. As such, during this time frame, the actuator should remain inflated and provide constant force, which is achieved by maintaining the linear actuator stationary. More details about this process can be found in the Appendix.

V. Psycophysical experiment

A. Participants

Five women and ten men with an average age of 25.33 years (standard deviation, SD: 2.18) participated in a psychophysical experiment. Only one participant was left-handed and none of them presented any visual or sensory-motor disabilities. Regarding ring size, only one participant used the small-sized ring, five used the medium-sized ring, and nine employed the large-sized ring. The experimental protocol was approved by TU Delft Human Research Ethics Committee (approval number 4546). All participants gave their informed consent.

B. Texture selection

An essential part of this study involves selecting appropriate textures to simulate out of the fifty surfaces included in the SENS3 database. The chosen textures should be suitable for rendering using the described techniques and exhibit distinct properties that participants can easily differentiate, but also

be challenging enough to keep the experimental procedure engaging.

To achieve this, we performed principal component analysis (PCA) on the texture adjective ratings from the SENS3 database. Following the method described by Balasubramanian et al. [28], we first normalized and then averaged the ratings for every participant, producing a matrix with fifty rows and eight columns, corresponding to the fifty textures and eight adjective pairs, respectively. After calculating the eigenvectors of the normalized covariance, roughness, compliance, temperature, and friction were identified as the four optimal dimensions that best represent the data. However, since our setup cannot render friction cues, we excluded this dimension, leaving us with three values representing the roughness, softness, and temperature of each texture.

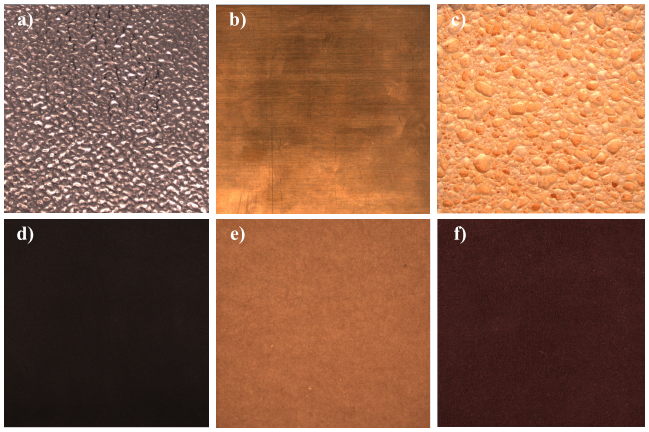

Fig. 6: Textures chosen for the psycophysical experiment: (a) rough metal, (b) smooth metal, (c) rough foam, (d) smooth foam, (e) cardboard, (f) fabric

These values allowed us to identify which of the fifty textures exhibited the most distinguishable parameters. We calculated the norm of each texture's roughness, softness, and temperature dimensions and selected the texture with the maximum norm in each quadrant, resulting in a list of eight surfaces. This approach enabled us to identify textures with unique combinations of properties, such as the surface with the highest roughness, softness, and temperature, or the one with the highest roughness and lowest softness and temperature, for instance.

After initial trials, we realized that eight textures led to an excessively long and complex experiment that could fatigue and confuse the participants. Therefore, we reduced the number to six, selecting those textures that demonstrated the best rendering and most distinct features when displayed by our ring. The final six selected textures, shown in Figure 6, are the following: rough metal, smooth metal, rough foam, smooth foam, cardboard, and fabric.

C. Texture validation

The next step of this work involves verifying that the selected rendering approaches are suitable for the chosen textures. To do this, we must confirm that the actuator's responses closely match the rendering signals.

In order to determine the rendering fidelity of the temperature signals, we compare the target temperature of the silicone tube display calculated using Ho and Jones' model with its actual temperature, measured using the miniature thermistor placed on top of the display.

While evaluating the thermal response of the actuator is a straightforward process using the same sensor that controls the thermal rendering process, measuring the actuator response for vibration and pressure signals is more challenging. Since our system does not include any sensor to measure the vibration or forces applied by the pneumatic chamber, a validation setup was designed. This setup consists of a 3D-printed cylinder with the same diameter as the ring, featuring a flat surface on one side to which a force-sensitive resistor (FSR-402) is attached. This sensor measures the force applied by the pneumatic actuator in response to the pressure and vibration signals. For pressure signals, we aim to determine the force magnitude that the actuator can generate. In contrast, for the vibration signals, our primary concern is not the force magnitude but ensuring that the pneumatic chamber inflates and deflates, and thus applies pressure, at the required times.

D. Experimental setup

During the experiment, each participant sat in front of a monitor and a set of six textures, as seen in Figure 7. Each of the textures was enclosed and hidden from view by a custom 3D-printed case. The cases had openings covered by a plastic layer that obscured the textures visually while still allowing participants to explore them freely by touch. To facilitate texture selection, each box was labeled with a number from one to six. Participants provided their responses through a graphical user interface (GUI) displayed on the monitor, using a computer mouse to interact with the system.

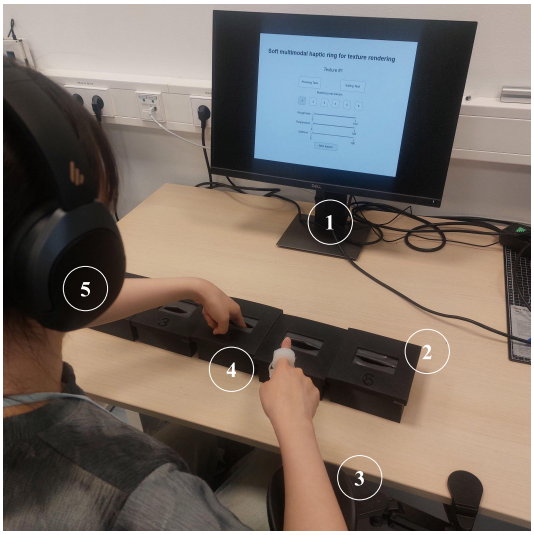

Fig. 7: Experimental setup: (1) monitor displaying GUI, (2) textures within 3D-printed enclosure, (3) arm rest, (4) soft multimodal haptic ring, (5) noise-cancelling headphones

Participants wore the custom-designed soft ring on the proximal phalanx of the index finger on their dominant hand. For added comfort, they could rest their dominant arm on an armrest positioned in front of the textures. Throughout the experiment, users wore noise-cancelling headphones (W830NB, Edifier) that played white noise to block auditory cues and minimize distractions.

E. Experimental procedure

Before the experiment began, each participant thoroughly washed their hands. After briefly explaining the study, they were asked to explore each of the displayed textures using the index finger of their dominant hand. They were asked to pay special attention to performing pressing, static contact and sliding lateral motions when exploring the surfaces. During this process, participants were presented with the first GUI, where they were asked to rate each texture on three dimensions: roughness, temperature, and softness. These dimensions were evaluated using the flat-bumpy, cold-hot and soft-stiff adjective pairs, respectively. Although employing the rough-smooth pair to rate roughness may seem more intuitive, preliminary trials showed that participants could be confused with surface friction, which our setup does not simulate. Therefore, we opted for the bumpy-flat rating, as it better describes the surface properties of the textures we are rendering.

After completing the first adjective rating stage, participants were fitted with the multimodal ring on the index finger of their dominant hand, always ensuring that the actuators were properly positioned and the sensing elements were securely in place. Once the participant was comfortable, the second part of the experiment began. During this stage, participants were presented with a GUI displaying two tasks: a pressing task and a sliding task. The pressing task simulates pressing and maintaining static contact with a surface for thirty seconds, while the sliding task simulates the lateral exploration of a surface at a speed of 5 cm/s for a total of ten seconds. To guide participants on the movement and speeds being simulated, the GUI displays a ball moving at the corresponding rates and directions. For the sliding task, the ball moves horizontally, while for the pressing task, the ball moves vertically, descending and then remaining stationary to represent static contact. To enhance the realism of the simulation, participants were instructed to mimic these movements with their ring-equipped index finger. Additionally, they were encouraged to continue exploring the real textures with their non-dominant hand as much as needed throughout the entire experiment.

Participants were instructed to start every texture trial with the sliding task. Upon pressing the corresponding button in the GUI, a five second countdown began, followed by the appearance of the moving ball on the screen and the start of the roughness simulation. After completing the sliding simulation, participants proceeded to the pressing task, where temperature and pressure cues were provided simultaneously. For this task, the countdown did not start immediately after pressing the button. Instead, a ”preparing” label appeared on the screen to indicate a preparation stage, during which the water and ring tube display were heated to the required initial temperature. Once this temperature was reached, the five second countdown began, followed by the appearance of the moving ball on the screen. As mentioned, during the preparation stage, water was pumped through the ring until the display reached the target temperature, causing users to feel some thermal cues before the simulation began. Participants were instructed to ignore these preliminary thermal stimuli and focus only on those felt during the simulation. Additionally, they were asked to disregard any vibrations or oscillations caused by the movement of water through the tube.

After completing both tasks, participants were asked to select the real surface that best matched the virtual texture. They also rated the perceived virtual stimuli using the previously mentioned adjective pairs. Both tasks were completed directly through the GUI. After submitting their responses, participants continued to the next texture, for which the same approach was repeated. In total, four rounds were conducted, displaying each texture once per round and accounting for a total of twenty-four trials per participant.

As explained, only roughness cues were provided during the sliding simulation, while both temperature and pressure cues were delivered during the pressing stage. This combination of modalities is intentional, as temperature perception is significantly heightened during static contact compared to dynamic exploration [38]. Additionally, this approach shortened simulation duration, as the preparation stage to heat the display to the required temperature was only necessary for one of the tasks.

VI. Results

A. Texture validation

Thermal rendering validation for each of the selected textures is shown in Figure D.1 in the Appendix, comparing the target surface temperature computed using Ho and Jones' model with the recorded actuator surface temperature. The results indicate that the ring can provide thermal stimuli close to the target temperature, with the mean difference between the target and recorded values across all six selected textures being less than 1 °C. The ring accurately simulates materials with stable temperature profiles, such as rough foam, fabric, and cardboard, with mean errors as low as 0.2627 °C, 0.4241 °C, and 0.2909 °C, respectively. In contrast, surfaces that experience a sharp temperature decrease, like rough and smooth metal, show greater errors reaching up to 2 °C.

Figure D.2 displays the signals used to render pressure stimuli with the corresponding pneumatic actuator force response. Similarly, Figure D.3 illustrates the pulse signal used for vibration rendering and the measured actuator force in response to said signal. Only a two-second interval of the vibration rendering is shown, which is repeated throughout the duration of the simulation.

B. Psycophysical experiment

The first round of displayed textures for each participant was excluded from data analysis, as its purpose was to familiarize

participants with the system and allow them to explore how different stimuli were perceived. Therefore, data analysis was conducted using only eighteen trials per participant, with three repetitions per texture.

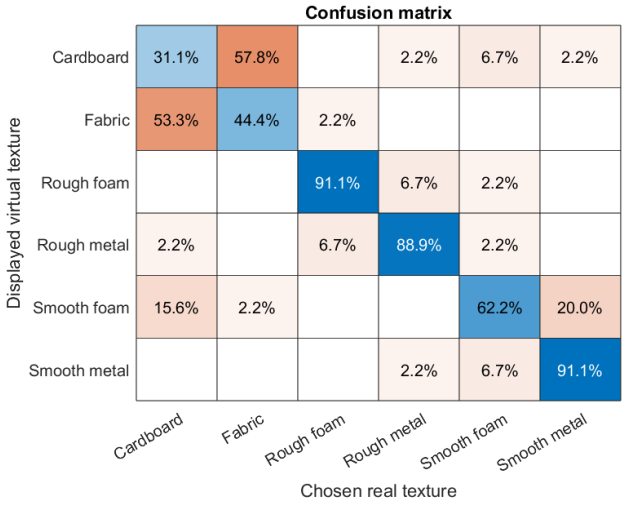

Fig. 8: Confusion matrix of the matching task, with the presented virtual textures as rows and the selected real textures as columns, where each cell shows the proportion of times each pair was chosen, and where the diagonal represents the expected correct answers.

Figure 8 presents the confusion matrix for the matching task, illustrating the relationship between the virtual textures displayed by the ring and the real textures selected by participants. A two-sample Pearson Chi-Squared test (χ^2 (25, N = 270) = 756, $p < 0.001$) was conducted, revealing that the distribution of participant predictions significantly deviates from what would be expected by chance (1/6 probability per texture). This finding indicates that participant responses were not random and that there is a significant association between the displayed virtual textures and the real textures chosen by participants.

Figure 9 displays the adjective ratings for the virtual textures, where roughness, temperature, and softness ratings for each texture are shown separately. We first applied a Kolmogorov-Smirnov test to assess the normality of each distribution. The test results indicate that the distributions deviate significantly from normality ($p < 0.05$). As a result, we applied a Kruskal-Wallis test to identify any statistically significant differences in adjective ratings across textures and modalities. The results of this analysis are presented in Figure 10 for roughness, temperature, and softness, respectively.

The findings suggest that for roughness ratings, there are no significant perceived differences between rough foam and rough metal, smooth metal and smooth foam, or cardboard and fabric. However, these groups exhibit statistically significant differences when compared to each other ($p < 0.001$). Regarding temperature ratings, metal textures were perceived to have similar temperature characteristics, as were the cardboard, fabric, and foam textures within their respective group. Notably, a statistically significant difference in temperature ratings was observed between the metal group and the other textures ($p < 0.001$). In terms of softness, rough foam was the only material that showed a statistically significant difference in softness compared to all other textures ($p < 0.001$). Additionally, smooth metal differed significantly in softness from smooth foam, fabric ($p < 0.05$), and cardboard ($p < 0.01$), while no significant differences were found in softness among the remaining textures.

Figure 11 compares the adjective ratings for virtual textures as displayed by the ring with those given at the start of the experiment when participants explored the textures freely with their fingertips. A Kolmogorov-Smirnov test indicated that the fingertip adjective ratings do not follow a normal distribution either ($p < 0.05$). Consequently, a non-parametric Mann-Whitney U test was conducted for each texture dimension to identify any significant differences between real and virtual adjective ratings. Test results indicate no significant difference in the perception of roughness between the real and virtual versions of rough foam ($p = 0.5859$, $p > 0.05$). Similarly, temperature ratings for virtual textures, including rough foam ($p = 0.2138$), smooth metal ($p = 0.0749$), fabric ($p = 0.7298$), cardboard ($p = 0.1707$), and smooth foam ($p = 0.2589$), did not significantly differ from their real counterparts ($p > 0.05$). In terms of softness, only the fabric texture showed no significant difference between its real and virtual representations ($p = 0.1329$, $p > 0.05$).

VII. Discussion

This study introduces an innovative soft wearable haptic interface that delivers multimodal stimuli to simulate textures. As such, our system effectively renders roughness, temperature, and compliance signals recorded during the tactile exploration of real textures with the fingertip. Results demonstrate that our device not only tracks these signals accurately but also achieves high precision in matching simulated textures to their real counterparts.

A. Texture validation

The proposed system accurately tracks target display temperatures, providing material-like thermal sensations. The device performs particularly well when simulating textures with relatively constant temperature profiles, as is the case of rough foam, fabric or cardboard. Instead, for textures that experience a sharper temperature decrease, the system shows greater error. This behaviour can be attributed to the character of the hydraulic system itself, which presents issues related to uneven water mixing, difficulties in maintaining exactly constant temperatures of the hot and cold tanks, and potential inaccuracies from thermistor placement, which may shift slightly due to tube oscillations and introduce noise. Although efforts were made to minimize these issues, the high specific heat capacity of water results in slow cooling processes, making delays an inherent part of our system, especially when rendering curves with sharp temperature drops.

In terms of pressure rendering, as expected, the real pressing data from bare finger interactions differs significantly

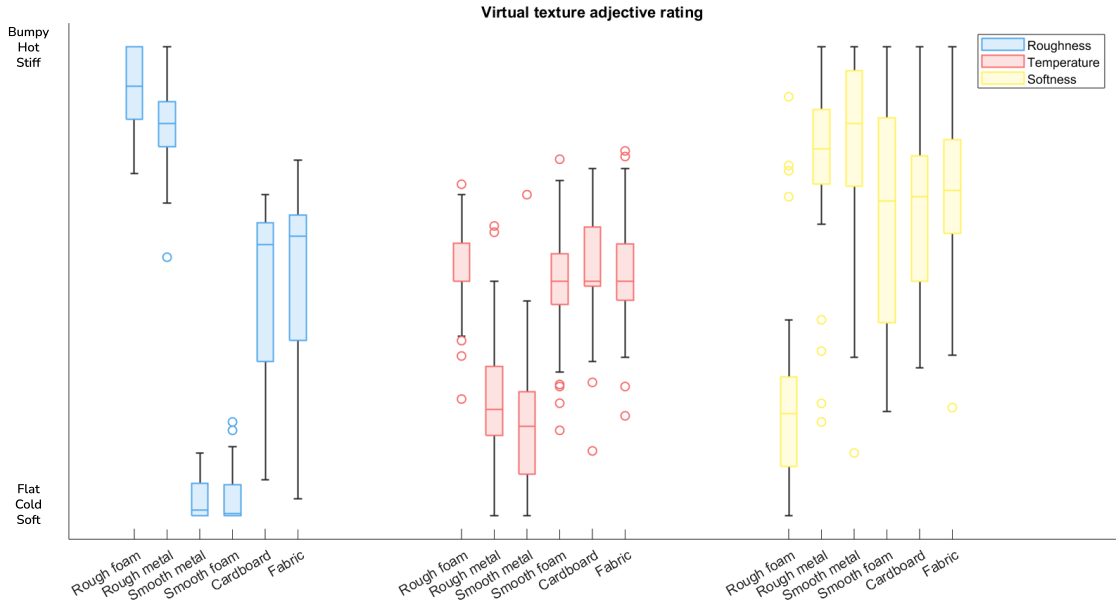

Fig. 9: Adjective ratings for each of the displayed virtual textures within their roughness, temperature and softness dimensions.

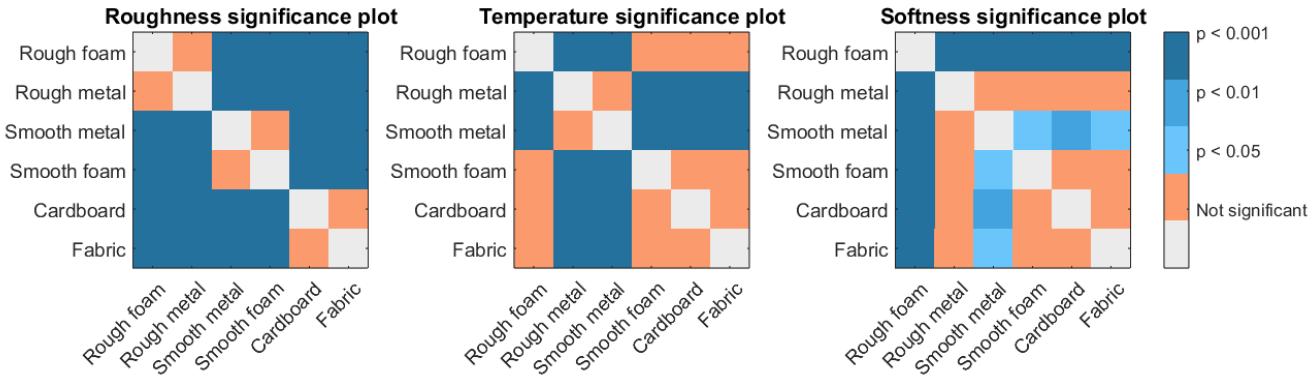

Fig. 10: Statistical significance plots for the roughness, temperature and softness dimensions of the displayed virtual textures, obtained after applying a Kruskal-Wallis test.

from both our rendering and experimentally measured signals. Nonetheless, our approach effectively generates force profiles that simulate different textures. In this way, as with the real interaction data, most materials exhibit similar force profiles, with the exception of rough foam, which shows much lower forces and slower inflation rates due to its airy, thick, and soft surface. While one might anticipate smooth foam to display a similar profile to rough foam, it actually behaves similarly to the other textures. This discrepancy is likely due to the texture samples themselves, as with the exception of rough foam, all the other textures are relatively thin and produce very similar compliance profiles.

In terms of tracking the pressure rendering signal, the ring actuator effectively simulates the inflation and deflation rates for each material. However, during the static contact phase of the simulation where a constant force is expected, most samples exhibit a decrease in force. We hypothesize that this decrease is due to the pneumatic chamber shifting slightly from its initial position against the sensor once airflow stops, causing a declining trend. Nevertheless, maximum force applied closely matches the rendering signal target force, with a difference of less than 0.5 N for most textures. This discrepancy is more pronounced for the rough foam and smooth metal, which is expected, as these surfaces are the softest and stiffest, and thus correspond to the linear actuator's maximum and minimum speed, leading to more extreme behaviours.

The vibration signal validation confirms that the actuator's force response accurately follows the target pulse signal. Al-

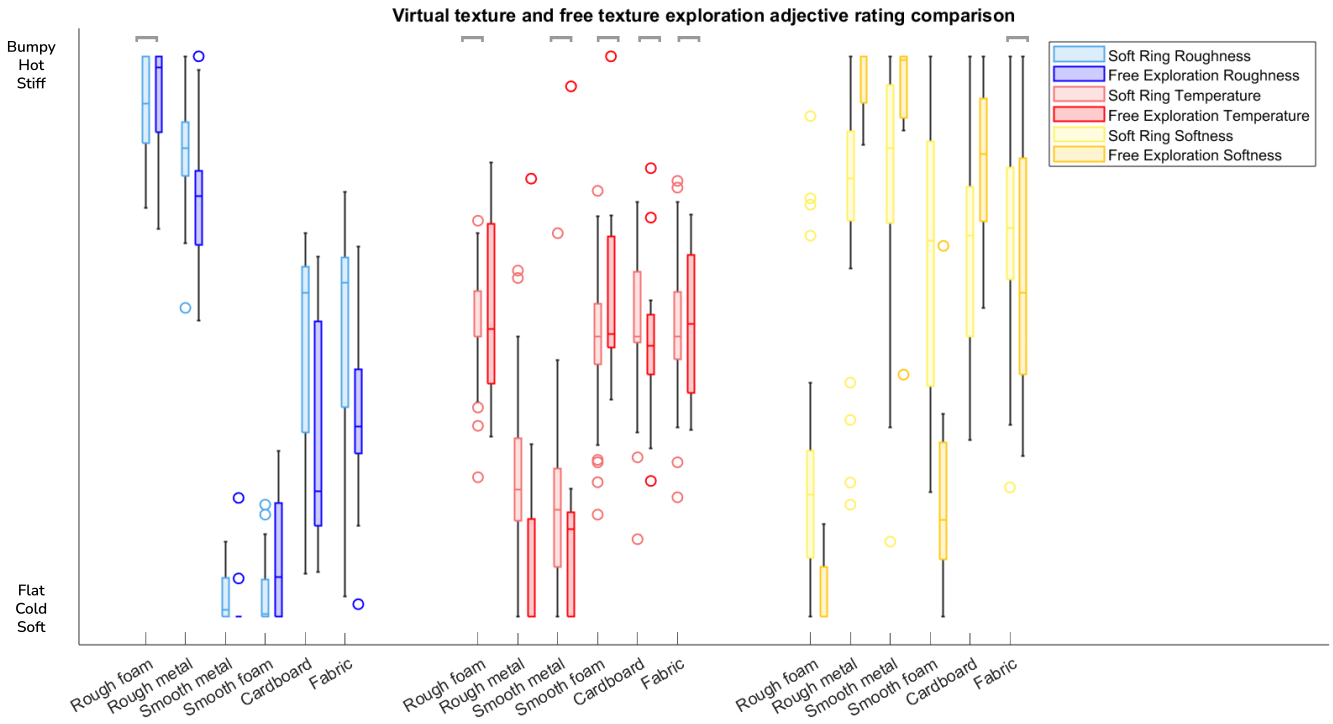

Fig. 11: Comparison between adjective ratings for the soft ring-displayed virtual textures (light) and the real freely explored textures (dark), for their roughness, temperature and softness dimensions, where brackets show pairs for which no statistical significant was found ($p > 0.05$).

though some delays are inevitable due to the time required for the actuator to inflate and deflate, the applied force increases when the valve is open and decreases to its minimum when the valve closes and air escapes the system. This behavior can be clearly observed for the rough foam and rough metal textures. For smooth foam and smooth metal, the force signal remains constant at its lowest state, as the valve remains closed and no air flows into the ring. Unexpectedly, fabric and cardboard textures also exhibit this constant force behaviour. This is however due to the limitations of our force sensor, as the actuator inflates and deflates very rapidly, applying small forces that our measurement setup cannot detect but that are clearly perceptible to the user.

B. Psycophysical experiment

Our confusion matrix indicates that the texture matching process was not random, as the correct matching rate for all textures was significantly higher than chance. Particularly, the rough foam, rough metal, and smooth metal textures achieved the highest accuracy, reaching up to 90%. Coincidentally, these textures also exhibited the most extreme PCA adjective ratings among our selected surfaces due to their distinct features in certain dimensions, such as temperature for metals, the bumpy surface of rough foam and metal, or the softness of rough foam. Soft foam, with a correct matching rate of 62.2 %, was more frequently misidentified than the previous textures, often mistaken with smooth metal and cardboard. This lower accuracy is likely due to the similar compliance profile of the soft foam to the stiffer textures. We suspect that confusion arose when participants rated the real soft foam as compliant but perceived a stiffer virtual texture, more akin to metals instead. As seen, fabric and cardboard textures show the poorest results, with fewer than 50 % correct guesses. While users could identify that the displayed texture was one of these two, distinguishing between them was largely done by chance. This outcome was anticipated, given that both textures exhibit very similar profiles across all dimensions, both in the actuator's rendering signals and in the real texture-recorded signals, as detailed in the Appendix.

Our virtual textures adjective ratings revealed the perception of three distinct roughness levels: rough foam and rough metal are rated as very bumpy, smooth foam and smooth metal are seen as very flat, and fabric and cardboard are perceived as having medium roughness. This finding aligns with our confusion matrix, where textures with similar roughness properties, such as cardboard and fabric or smooth foam and smooth metal, were often misidentified. In terms of temperature, two distinct levels, cold and medium temperature, were perceived. Metals were easily distinguishable due to their colder temperature profile, while the other materials were perceived as having similar profiles close to room temperature. Regarding softness, only the rough foam texture was rated as very soft, while the other textures were described as quite stiff. Interestingly, smooth metal, identified as the stiffest material in our PCA,

was also rated as the most stiff virtual texture in our adjective ratings.

When comparing our virtual textures' adjective ratings to those of real textures, the temperature dimension showed the most accurate results. For all virtual textures except rough metal, the perceived temperature closely matched that of their real counterparts. In contrast, the roughness and softness dimensions were more limited, with matches only observed in the bumpiness of rough foam and the compliance characteristics of fabric.

These results indicate that our temperature rendering approach was the most accurate, which is unsurprising given that Ho and Jones' rendering algorithm has been extensively studied. In contrast, our roughness and compliance models involve important simplifications, leading to the greater disparities in their adjective comparison to real textures. Nevertheless, our study also revealed that the chosen temperature rendering approach has significant limitations, as it does not take into consideration the actual temperature of the skin. Although the model uses previously recorded skin temperature data, it does not account for the participant's initial skin temperature, which can vary significantly based on factors such as age [39], gender [40] or ambient temperature [41]. For instance, since our experiment was conducted in August, with room temperatures reaching up to 29°C on several days, participants' skin temperatures may have been elevated, which led to the rating of many thermal cues as close to room temperature. Participants reported this effect after the experiment, noting that while cold temperatures were easy to perceive, other thermal stimuli were harder to detect and feel. To address this limitation, we propose adjusting the target display temperature computed by Ho and Jones' model to align initially with the participant's skin temperature. It is however also possible that such an adjustment may not significantly improve temperature perception, as the issue might be linked to our ring itself. In this way, as our ring inflates and compresses the finger, it may reduce blood flow to the area, thereby diminishing temperature sensitivity. This effect could have been exacerbated by our ring design, which places the temperature presenting system directly opposite to the pneumatic actuator.

In terms of roughness, although the adjective ratings for real and virtual textures aligned for only one of the surfaces, we believe that results indicate that our image rendering algorithm is a viable approach. It is likely that a more traditional roughness rendering algorithm based on sliding forces or accelerations might have produced adjective ratings more closely matching those of real textures, however, given the limitations of our pneumatic valve, our roughness rendering system successfully provided distinguishable levels of roughness that corresponded well to real textures. Interestingly, participants reported that roughness was their preferred modality, describing it as particularly prominent, realistic, and easy to distinguish. Many participants noted that they primarily relied on roughness cues for texture matching, which is consistent with previous research indicating that roughness is one of the most critical dimensions of touch [42].

Comparatively, the softness dimension yielded worse results. This behaviour was anticipated, given the limitations of our pneumatic system and rendering algorithm which significantly simplifies compliance signals. Nonetheless, participants were able to clearly distinguish between very soft and stiff materials. It is however possible that, even if the original compliance signals had been rendered perfectly, similar results might have been obtained due to the similar profiles exhibited by most textures. This results suggest that compliance is not only related to applied force but also to indentation depth, surface geometry and contact area [43], factors that were not considered when designing our system.

Overall, our results highlight the critical role of multimodality in haptic perception. In fact, participants described the importance of experiencing all three haptic modalities before they could accurately match the perceived cues to a real texture. They indicated that matching textures without one of these modalities would have been significantly more difficult. Our experiment also marked the importance of the thermal dimension in haptics, with many participants reporting relying more on temperature stimuli than on softness cues. We believe that thermal cues contribute significantly to the realism of texture simulation, as participants who did not perceive thermal cues as clearly tended to describe the texture simulation as less immersive. This was particularly evident in the case of one participant with a small scar near the temperature presenting area, who described the experience as more of a "pattern matching" task rather than a realistic simulation. These findings suggest the need for the development of smaller, wearable and flexible thermal displays, as this dimension has often been overlooked in haptic devices.

Additionally, our experiment demonstrates that haptic cues can be effectively relocated from the fingertip to the phalanx. While it is likely that certain stimuli would have been more distinctly perceived at the fingertip, especially thermal and softness cues which often present only subtle differences between textures, participants were still able to perceive and differentiate cues. Stimuli were matched to real textures with notable accuracy, thereby proving the feasibility of relocating haptic cues from the fingertip to other parts of the finger.

C. Limitations and future research

Despite careful device and experimental design, our work presents some limitations. As such, even though we produced rings of three different sizes to accommodate various finger types, the fit was not always perfect, being slightly too tight or too loose for some participants, which may have particularly affected pressure and temperature perception. Additionally, despite our efforts to ensure consistent inflation characteristics across all rings, minor variations in the manufacturing process could have introduced small differences in performance.

Our experimental procedure also has limitations, particularly regarding temperature rendering. As discussed, before the simulation begins, water needs to be pumped through the ring, which may have unintentionally influenced participants' perceptions, even though they were instructed to focus only

on the temperature cues felt once the simulation started. Additionally, vibrations from the pump during water circulation, although participants were asked to disregard them, could have been confusing or distracting. Another significant limitation of our hydraulic system is the need for constant monitoring of water temperatures. For instance, adding ice to the cold tank was occasionally necessary, which may have affected participant perceptions. In terms of our pneumatic system, noise generated by the pneumatic valve presented an issue. Despite efforts to mitigate this problem by having participants wear noise-canceling headphones, it is possible that some sound was perceived, potentially influencing participants' roughness perception.

Moreover, our texture assessment results are constrained by the use of an adjective rating approach based on the semantic differential method, where participants rated materials using a scale of opposing adjective pairs. Despite our best efforts to select the adjective pairs that best capture our rendering modalities, they may not have been representative for some participants. Furthermore, it is possible that some participants' ratings were influenced by the real textures they were touching, especially for those dimensions that were less clearly perceived.

Finally, the greatest limitation of our system is its size and complexity. Although the ring is wearable, soft, small, lightweight, and flexible, it requires large, complex, and bulky circuits to operate, which significantly restricts its usability and application. Despite our encouraging results, we believe that simplifying the system is essential, even if it is at the detriment of our design's soft and flexible character. As such, we recommend future versions of the system to replace the hydraulic circuit by a Peltier cell that provides thermal cues. We recommend enclosing this element within a silicone layer to reduce its stiffness and integrate better within the ring. Alternatively, flexible thermal interfaces, such as the one developed by Lee et al. [44], which combines heating and cooling functions while maintaining softness could be used. Additionally, for a more compact version of the device, we suggest replacing the air compressor with a portable system based on small air cartridges, as illustrated by Talhan et al. [13]. We believe these modifications would lead to a more wearable system with improved control, enhancing its applicability and practicality.

VIII. Conclusion

This paper presents the design of a novel soft multimodal haptic ring targeted for texture rendering. We successfully demonstrated that our system can, not only provide various types of feedback, but can also simulate the thermal, roughness and compliance properties of real textures with high accuracy and performance. Moreover, our ring, made entirely of soft materials, ensures maximum comfort and adapts well to the flexible nature of the skin while relocating stimuli from the fingertip. Based on our results we can conclude the following:

- To the best of our knowledge, this is the first soft multimodal wearable ring capable of providing pressure, thermal, and vibratory cues independently. Furthermore, it is the first soft interface designed to render real textural signals acquired from free fingertip exploration.
- The device simulates real textures with high accuracy, achieving virtual-to-real matching rates of up to 90 % for several surfaces.
- Our device successfully provides cues that are perceived as distinctly different across all three rendered perceptual dimensions. Additionally, no significant differences were observed in the evaluation of real and virtual modalities across several of the selected textures.

In this way, we believe that our ring holds great promise for future applications, particularly in the fields of mixed and augmented reality. We argue that such a multimodal wearable interface that provides realistic simulations while allowing full range of motion and free environment exploration could be revolutionary within the haptics field.

References

[1] A. R. See, J. A. G. Choco, and K. Chandramohan, "Touch, texture and haptic feedback: A review on how we feel the world around us," *Applied Sciences*, vol. 12, no. 9, 2022.

[2] B. Hannaford and A. M. Okamura, *Haptics*, pp. 1063–1084. Cham: Springer International Publishing, 2016.

[3] A. El Saddik, "The potential of haptics technologies," *IEEE Instrumentation Measurement Magazine*, vol. 10, no. 1, pp. 10–17, 2007.

[4] B. L. Kodak and Y. Vardar, "Feelpen: A haptic stylus displaying multimodal texture feels on touchscreens," *IEEE/ASME Transactions on Mechatronics*, vol. 28, no. 5, pp. 2930–2940, 2023.

[5] D. Chen, A. Song, L. Tian, Y. Yu, and L. Zhu, "Mh-pen: A pen-type multi-mode haptic interface for touch screens interaction," *IEEE Transactions on Haptics*, vol. 11, no. 4, pp. 555–567, 2018.

[6] J. Yin, R. Hinchet, H. R. Shea, and C. Majidi, "Wearable soft technologies for haptic sensing and feedback," *Advanced Functional Materials*, vol. 31, 2020.

[7] X. Gu, Y. Zhang, W. Sun, Y. Bian, D. Zhou, and P. O. Kristensson, "Dexmo: An inexpensive and lightweight mechanical exoskeleton for motion capture and force feedback in vr," in *Proceedings of the 2016 CHI Conference on Human Factors in Computing Systems*, CHI '16, (New York, NY, USA), p. 1991–1995, Association for Computing Machinery, 2016.

[8] C. Pacchierotti, D. Prattichizzo, and K. J. Kuchenbecker, "Displaying sensed tactile cues with a fingertip haptic device," *IEEE Transactions on Haptics*, vol. 8, no. 4, pp. 384–396, 2015.

[9] C. Gaudeni, L. Meli, L. A. Jones, and D. Prattichizzo, "Presenting surface features using a haptic ring: A psychophysical study on relocating vibrotactile feedback," *IEEE Transactions on Haptics*, vol. 12, no. 4, pp. 428–437, 2019.

[10] C. Pacchierotti, G. Salvietti, I. Hussain, L. Meli, and D. Prattichizzo, "The hring: A wearable haptic device to avoid occlusions in hand tracking," in *2016 IEEE Haptics Symposium (HAPTICS)*, pp. 134–139, 2016.

[11] H. A. J. van Riessen and Y. Vardar, "Relocating thermal stimuli to the proximal phalanx may not affect vibrotactile sensitivity on the fingertip," 2023.

[12] Z. Sun, M. Zhu, X. Shan, and C. Lee, "Augmented tactile-perception and haptic-feedback rings as human-machine interfaces aiming for immersive interactions," *Nature Communications*, vol. 13, no. 1, 2022.

[13] A. Talhan, H. Kim, and S. Jeon, "Tactile ring: Multi-mode finger-worn soft actuator for rich haptic feedback," *IEEE Access*, vol. 8, pp. 957–966, 2020.

[14] T. Han, F. Anderson, P. Irani, and T. Grossman, "Hydroring: Supporting mixed reality haptics using liquid flow," pp. 913–925, 10 2018.

[15] M. S. Hashem, J. B. Joolee, W. Hassan, and S. Jeon, "Soft pneumatic fingertip actuator incorporating a dual air chamber to generate multi-mode simultaneous tactile feedback," *Applied Sciences*, vol. 12, no. 1, 2022.

[16] B. Zhang and M. Sra, "Pneumod: A modular haptic device with localized pressure and thermal feedback," in *Proceedings of the 27th ACM Symposium on Virtual Reality Software and Technology*, VRST '21, (New York, NY, USA), Association for Computing Machinery, 2021.
[17] Y. Liu, S. Nishikawa, Y. Seong, R. Niiyama, and Y. Kuniyoshi, "Thermocaress: A wearable haptic device with illusory moving thermal stimulation," pp. 1–12, 05 2021.
[18] A. Talhan, S. Kumar, H. Kim, W. Hassan, and S. Jeon, "Multi-mode soft haptic thimble for haptic augmented reality based application of texture overlaying," *Displays*, vol. 74, p. 102272, 2022.
[19] M. Gabardi, D. Leonardis, M. Solazzi, and A. Frisoli, "Development of a miniaturized thermal module designed for integration in a wearable haptic device," in *2018 IEEE Haptics Symposium (HAPTICS)*, pp. 100–105, 2018.
[20] L. Massari, J. D'Abbraccio, L. Baldini, F. Sorgini, G. A. Farulla, P. Petrovic, E. Palermo, and C. M. Oddo, "Neuromorphic haptic glove and platform with gestural control for tactile sensory feedback in medical telepresence applications," in *2018 IEEE International Symposium on Medical Measurements and Applications (MeMeA)*, pp. 1–6, 2018.
[21] S. Weinstein, "Tactile sensitivity of the phalanges," *Perceptual and Motor Skills*, vol. 14, p. 351–354, June 1962.
[22] R. S. Johansson, "Tactile sensibility in the human hand: receptive field characteristics of mechanoreceptive units in the glabrous skin area.," *The Journal of Physiology*, vol. 281, p. 101–125, Aug. 1978.
[23] R. Wakolbinger, A. D. Roche, T. Stockinger, B. Gustorff, and O. C. Aszmann, "Multiregion thermal sensitivity mapping of the hand," *Journal of Plastic, Reconstructive amp; Aesthetic Surgery*, vol. 67, p. 1541–1547, Nov. 2014.
[24] R. H. Taus, J. C. Stevens, and L. E. Marks, "Spatial localization of warmth," *Perception amp; Psychophysics*, vol. 17, p. 194–196, Mar. 1975.
[25] B. G. Green, "Localization of thermal sensation: An illusion and synthetic heat," *Perception amp; Psychophysics*, vol. 22, p. 331–337, July 1977.
[26] R. Rameshwar, E. H. Skorina, and C. D. Onal, "Fabric-silicone composite haptic muscles for sensitive wearable force feedback," PETRA '23, (New York, NY, USA), p. 33–41, Association for Computing Machinery, 2023.
[27] H. Choi, S. Cho, S. Shin, H. Lee, and S. Choi, "Data-driven thermal rendering: An initial study," in *2018 IEEE Haptics Symposium (HAPTICS)*, pp. 344–350, 2018.
[28] J. K. Balasubramanian, B. L. Kodak, and Y. Vardar, "Sens3: Multisensory database of finger-surface interactions and corresponding sensations," 2024.
[29] H. H. Pennes, "Analysis of tissue and arterial blood temperatures in the resting human forearm," *Journal of Applied Physiology*, vol. 85, p. 5–34, July 1998.
[30] H.-N. Ho and L. Jones, "Thermal model for hand-object interactions," in *2006 14th Symposium on Haptic Interfaces for Virtual Environment and Teleoperator Systems*, pp. 461–467, 2006.
[31] H.-N. Ho and L. A. Jones, "Modeling the thermal responses of the skin surface during hand-object interactions," *Journal of Biomechanical Engineering*, vol. 130, Mar. 2008.
[32] L. A. Jones and H.-N. Ho, "Warm or cool, large or small? the challenge of thermal displays," *IEEE Transactions on Haptics*, vol. 1, no. 1, pp. 53–70, 2008.
[33] Intertronics, "Thermally conductive silicones." https://www.intertronics.co.uk/wp-content/uploads/2016/11/TB2007-12-Thermally-Conductive-Silicones.pdf, 2007.
[34] H. Culbertson, J. Unwin, and K. J. Kuchenbecker, "Modeling and rendering realistic textures from unconstrained tool-surface interactions," *IEEE Transactions on Haptics*, vol. 7, no. 3, pp. 381–393, 2014.
[35] Y. Vardar, A. İşleyen, M. K. Saleem, and C. Basdogan, "Roughness perception of virtual textures displayed by electrovibration on touch screens," in *2017 IEEE World Haptics Conference (WHC)*, pp. 263–268, 2017.
[36] R. F. Friesen and Y. Vardar, "Perceived realism of virtual textures rendered by a vibrotactile wearable ring display," *IEEE Transactions on Haptics*, vol. 17, no. 2, pp. 216–226, 2024.
[37] MathWorks, *Find Local Maxima - MATLAB findpeaks*, 2024. https://nl.mathworks.com/help/signal/ref/findpeaks.html.
[38] L. Peters, G. Serhat, and Y. Vardar, "Thermosurf: Thermal display technology for dynamic and multi-finger interactions," *IEEE Access*, vol. 11, pp. 12004–12014, 2023.
[39] P. R. Hernandes Júnior and A. V. Sardeli, "The effect of aging on body temperature: A systematic review and meta- analysis," *Current Aging Science*, vol. 14, p. 191–200, Dec. 2021.
[40] H. Zhang and L. Shen, "Effect of gender and body part differences on skin temperature and bed micro-environment during sleep in a moderate temperature environment," *Energy and Buildings*, vol. 297, p. 113459, Oct. 2023.
[41] D. R. HODGSON, *Thermoregulation*, p. 108–124. Elsevier, 2014.
[42] S. Okamoto, H. Nagano, and Y. Yamada, "Psychophysical dimensions of tactile perception of textures," *IEEE Transactions on Haptics*, vol. 6, no. 1, p. 81–93, 2013.
[43] C. Dhong, R. Miller, N. B. Root, S. Gupta, L. V. Kayser, C. W. Carpenter, K. J. Loh, V. S. Ramachandran, and D. J. Lipomi, "Role of indentation depth and contact area on human perception of softness for haptic interfaces," *Science Advances*, vol. 5, Aug. 2019.
[44] J. Lee, H. Sul, W. Lee, K. R. Pyun, I. Ha, D. Kim, H. Park, H. Eom, Y. Yoon, J. Jung, D. Lee, and S. H. Ko, "Stretchable skin-like cooling/heating device for reconstruction of artificial thermal sensation in virtual reality," *Advanced Functional Materials*, vol. 30, 02 2020.

A

Device concept and design

A.1. Ring fabrication

The technical drawings of the molds used to manufacture the rings can be found in the following pages. The schematics for the three different ring sizes are included. Each of the ring molds is divided into two pieces, upper and lower, that fit together for easier demolding.

A.2. Pneumatic circuit

The schematic below explains the operation of our pneumatic circuit to generate vibration and pressure cues, respectively, highlighting the state of each valve to permit or stop airflow.

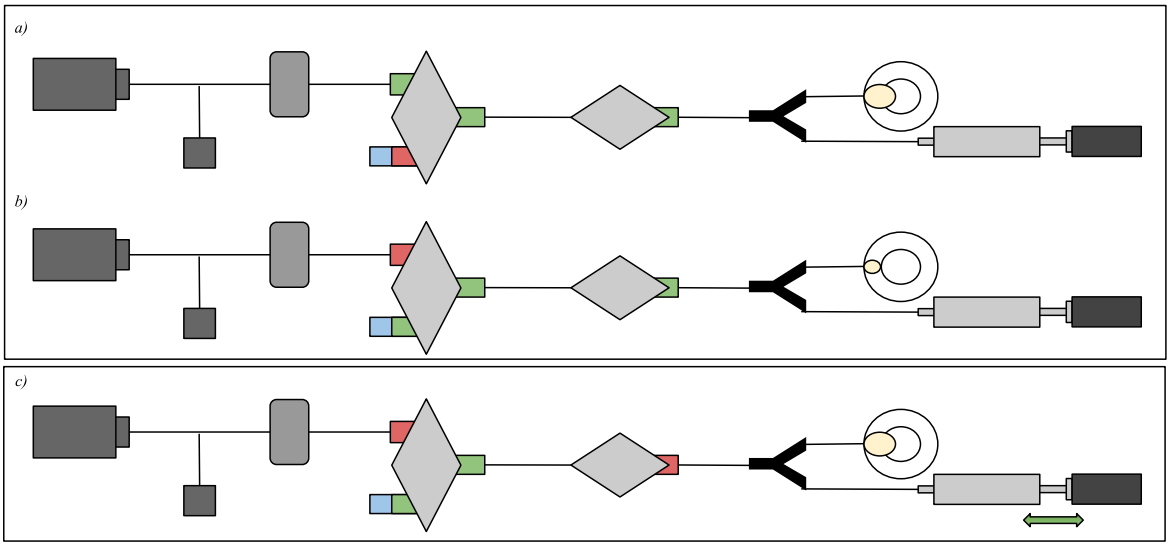

Figure A.1: Schematic showing the operation of the pneumatic circuit to provide vibration stimuli (a, b), and pressure cues (c), where the ports shown in green are open and those in red are closed.

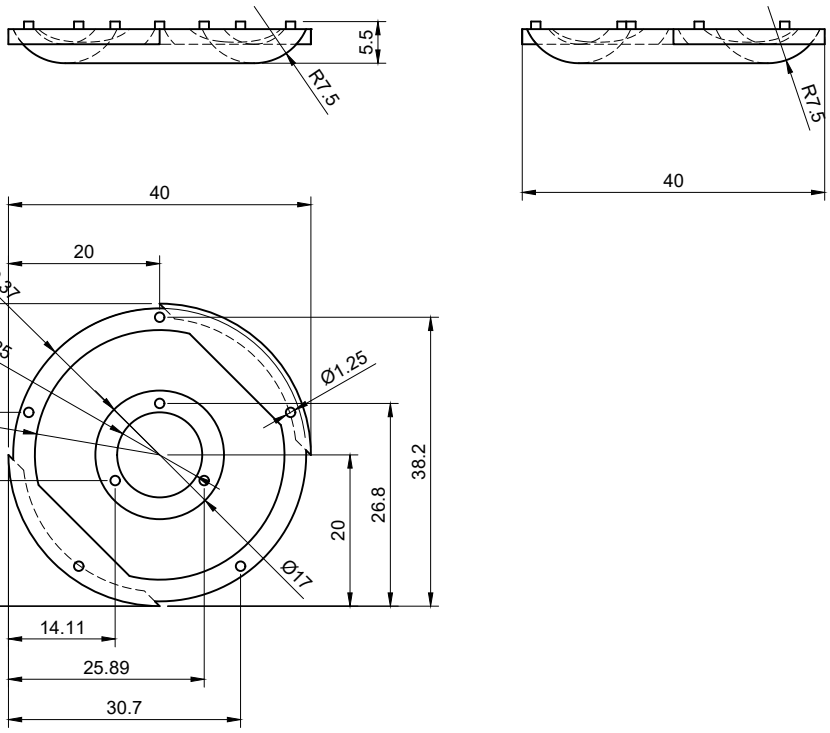

Dept.	Technical reference	Created by	Approved by
		Ana Sanz 12/08/2024	
		Document type	Document status
		Title: Size S Lower	DWG No.
			Rev. / Date of issue / Sheet: 1/2

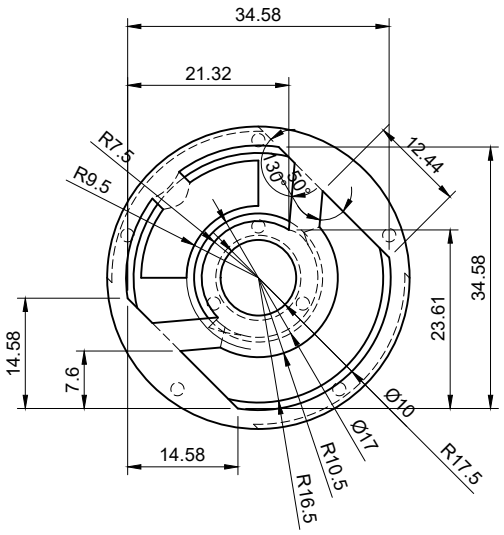

Dept.	Technical reference	Created by Ana Sanz 12/08/2024	Approved by
		Document type	Document status
		Title: Size S Upper	DWG No.
			Rev. / Date of issue / Sheet 2/2

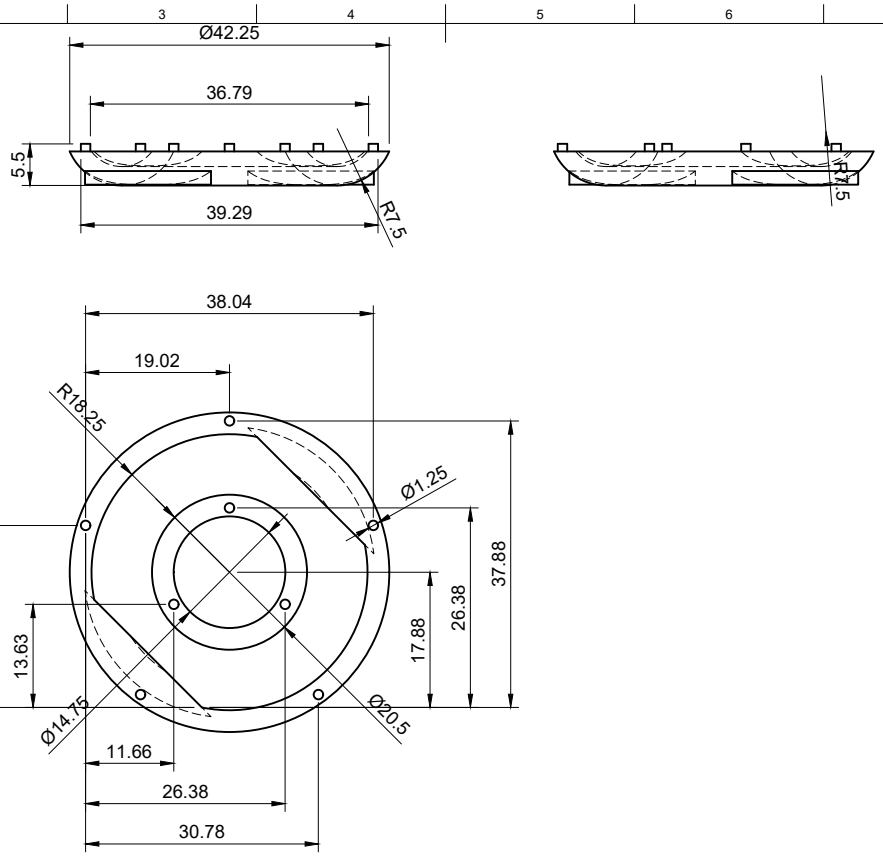

Dept.	Technical reference	Created by	Approved by
		Ana Sanz 12/08/2024	
		Document type	Document status
		Title: Size M Lower	DWG No.
			Rev. / Date of issue / Sheet: 1/2

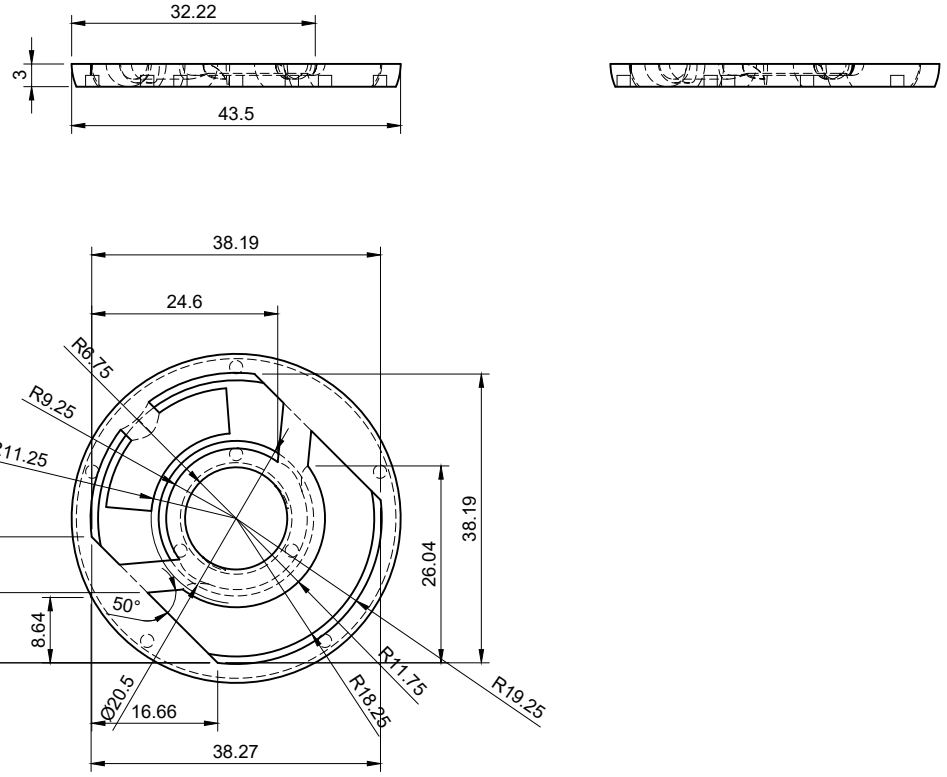

Dept.	Technical reference	Created by	Approved by
		Ana Sanz 12/08/2024	
		Document type	Document status
		Title: Size M Upper	DWG No.
			Rev. / Date of issue / Sheet: 2/2

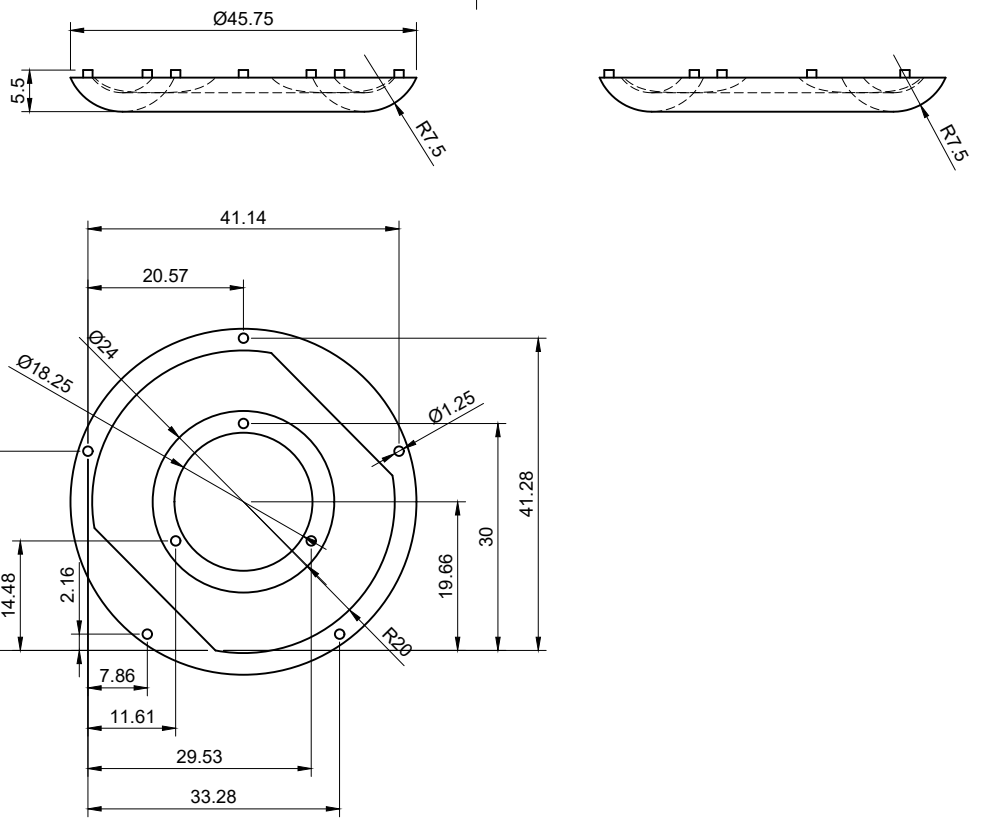

Dept.	Technical reference	Created by	Approved by
		Ana Sanz 12/08/2024	
		Document type	Document status
		Title: Size L Lower	DWG No.
			Rev. / Date of issue / Sheet: 1/2

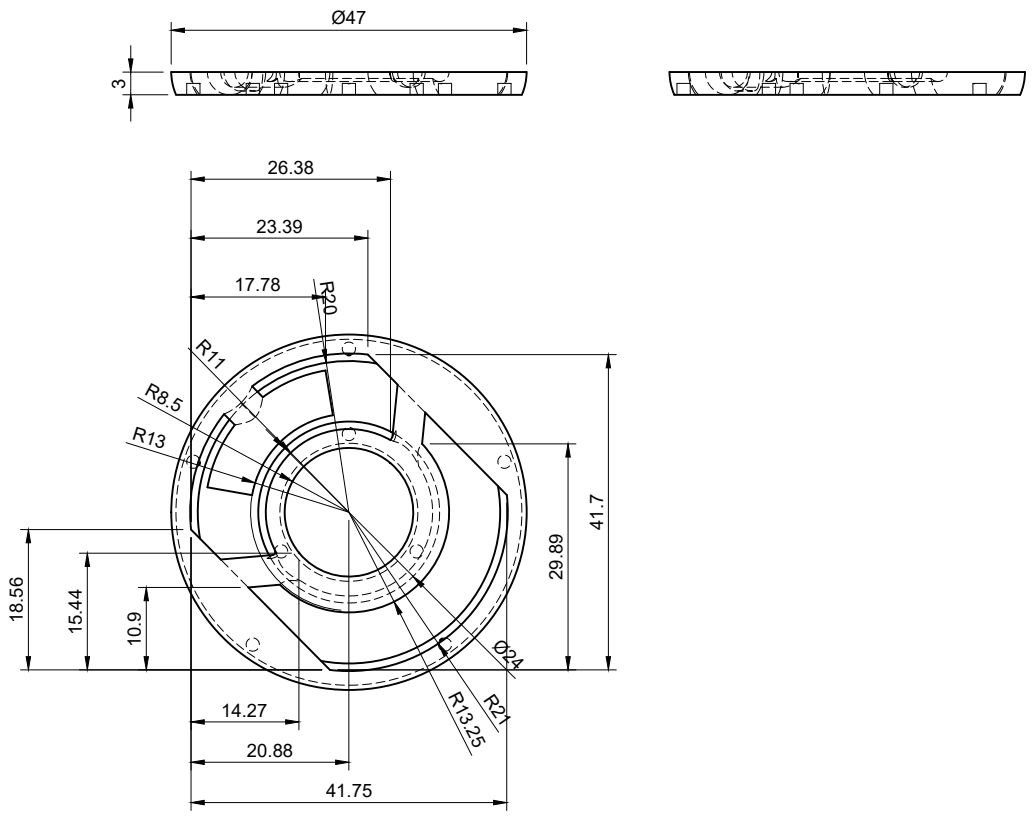

Dept.	Technical reference	Created by	Approved by
		Ana Sanz 12/08/2024	
		Document type	Document status
		Title: Size L Upper	DWG No.
			Rev. / Date of issue / Sheet: 2/2

B

Texture Rendering

B.1. Temperature rendering

The figures below illustrate the steps involved in generating the thermal signals sent to the microcontroller. The process starts with the SENS3 database, where skin temperature and heat flux signals are obtained. These signals are then filtered and cropped to isolate the period of finger contact. Next, the target thermal display temperature is calculated using Ho and Jones' model and is then fitted to a seventh-order polynomial.

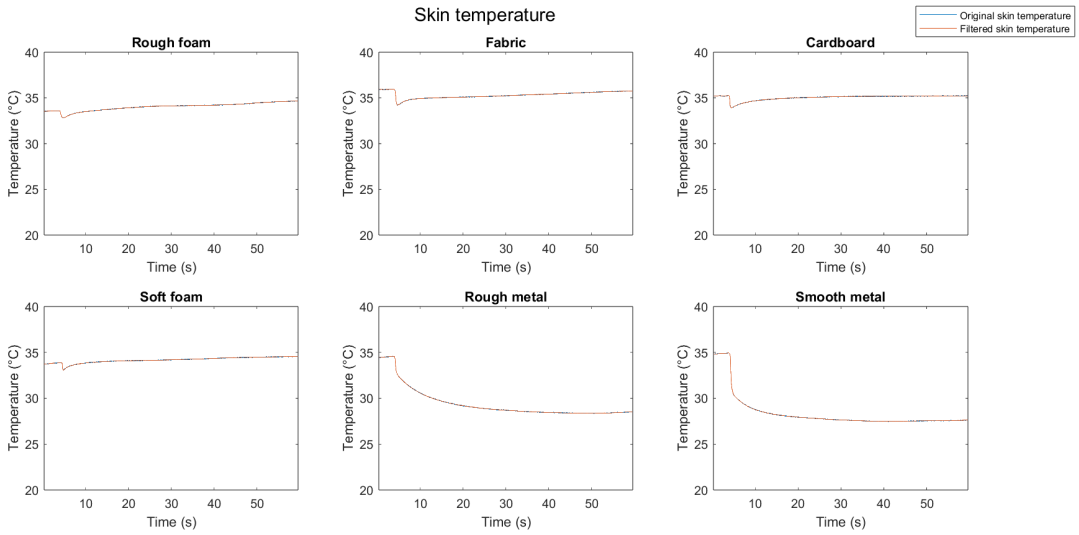

Figure B.1: Original and filtered skin temperature data from SENS3 database for the selected textures.

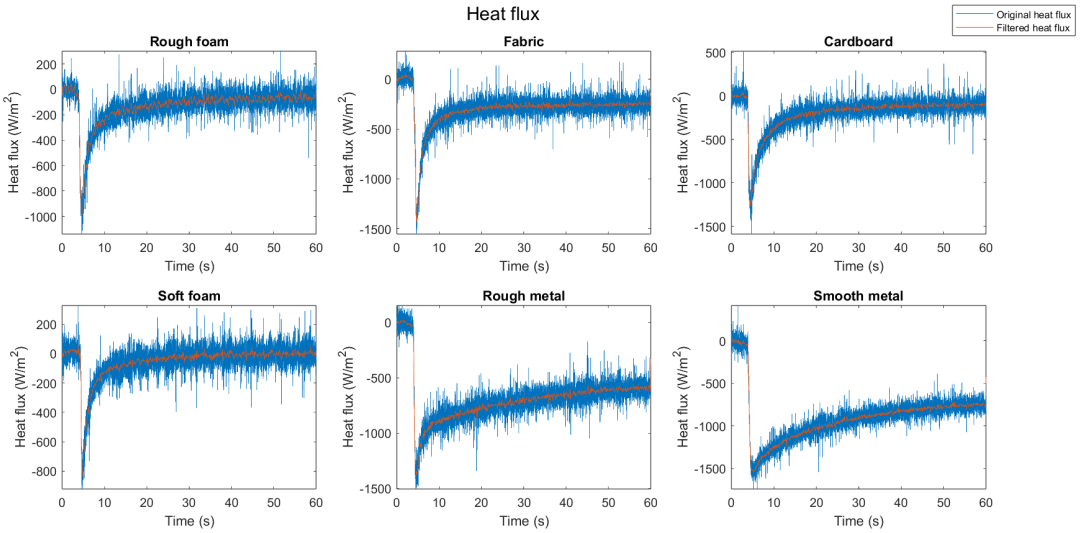

Figure B.2: Original and filtered heat flux data from SENS3 database for the selected textures.

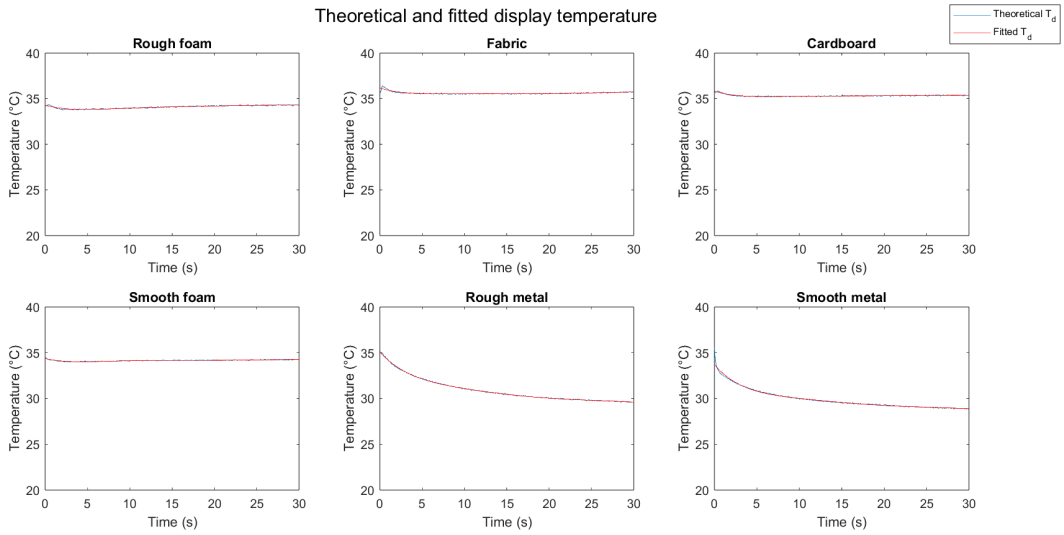

Figure B.3: Theoretical and fitted display temperature starting at time of contact for the selected textures.

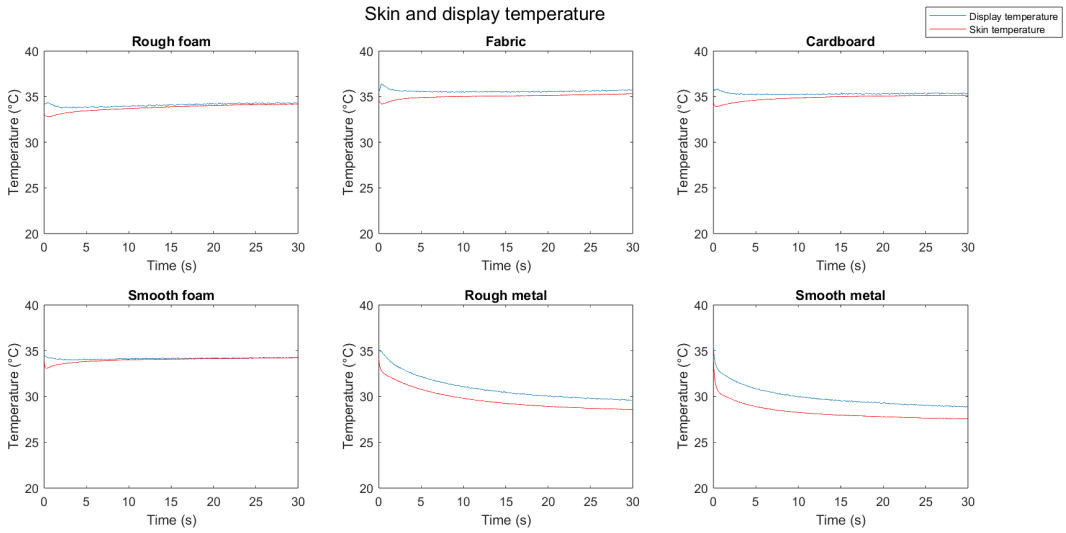

Figure B.4: Skin and display temperature starting at the time of contact for the selected textures.

Texture	Fitting Polynomial
Rough foam	$3.0020\times10^{-8}x^7 - 3.5617\times10^{-6}x^6 + 0.0001x^5 - 0.0039x^4 + 0.048x^3 - 0.2542x^2 + 34.28283$
Fabric	$3.0691\times10^{-8}x^7 - 3.7032\times10^{-6}x^6 + 0.0002x^5 - 0.0041x^4 + 0.0489x^3 - 0.2879x^2 + 36.1738$
Cardboard	$2.9928\times10^{-8}x^7 - 3.6020\times10^{-6}x^6 + 0.0002x^5 - 0.0040x^4 + 0.0486x^3 - 0.2790x^2 + 35.8213$
Smooth foam	$2.8751\times10^{-8}x^7 - 3.4706\times10^{-6}x^6 + 0.0002x^5 - 0.0037x^4 + 0.0424x^3 - 0.2043x^2 + 34.3522$
Rough metal	$6.1402\times10^{-8}x^7 - 7.4351\times10^{-6}x^6 + 0.0004x^5 - 0.0087x^4 + 0.1197x^3 - 1.0106x^2 + 35.0836$
Smooth metal	$7.3703\times10^{-8}x^7 - 8.9357\times10^{-6}x^6 + 0.0004x^5 - 0.0105x^4 + 0.1398x^3 - 1.0623x^2 + 33.6811$

Table B.1: Fitting seventh order polynomial for each of the selected textures.

B.2. Roughness rendering

The following figures outline the process used to generate binary pulse signals for rendering roughness. The process begins with top-view texture images, which are first converted to grayscale and then mean-filtered. A line of pixels spanning the entire image is selected, and the intensity along the line is plotted. The *findpeaks* algorithm is applied to identify the locations of peaks and valleys, corresponding to the events when the valve should be turned off and on. Finally, the signal is converted into a time-based signal.

As shown in Figure B.8, our algorithm effectively detects peaks and valleys in very rough and smooth textures, producing accurate roughness signals. However, for finer surfaces like fabric and cardboard, our approach struggles to detect small peaks, leading to overly simplified signals that are either too bumpy or too smooth, as illustrated in Figure B.9. To address this issue, the rendering signal for these surfaces was replaced with a 300 Hz square binary signal, as depicted in Figure B.10.

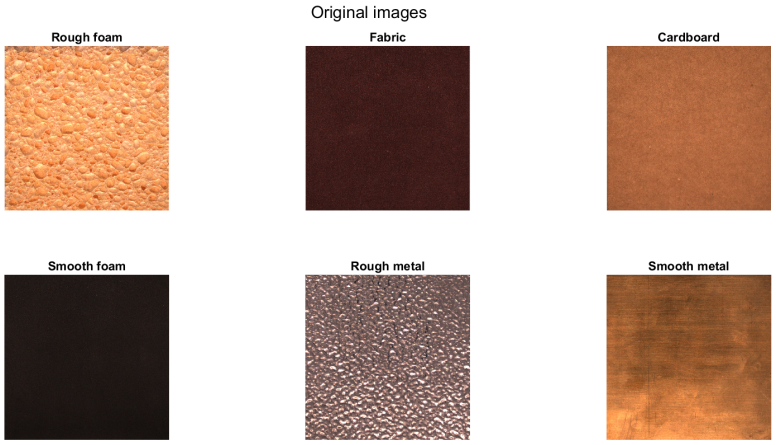

Figure B.5: Original top-view surface images for each of the selected textures.

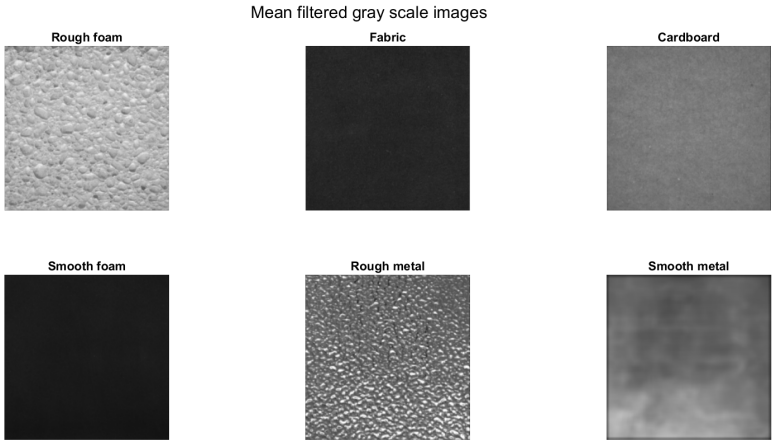

Figure B.6: Grayscaled and mean-filtered surface images for each of the selected textures.

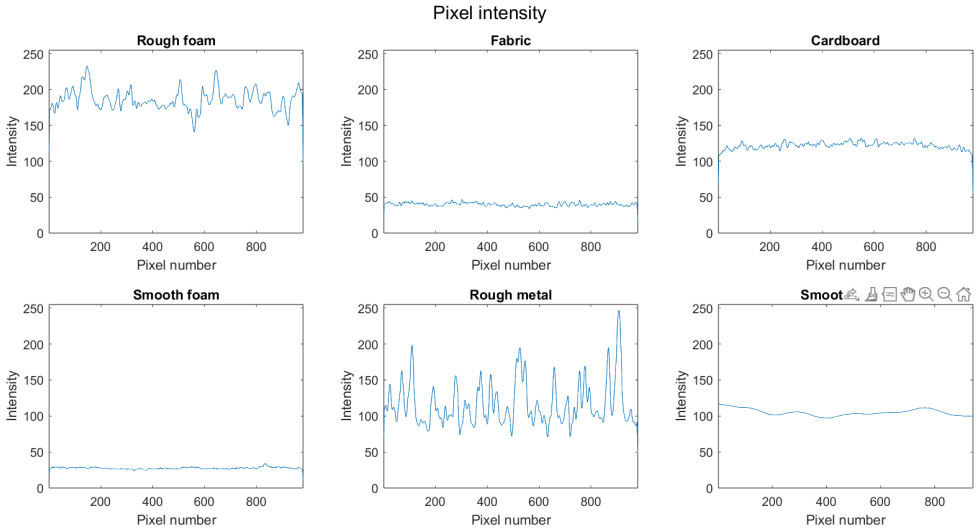

Figure B.7: Pixel intensity for each of the selected images.

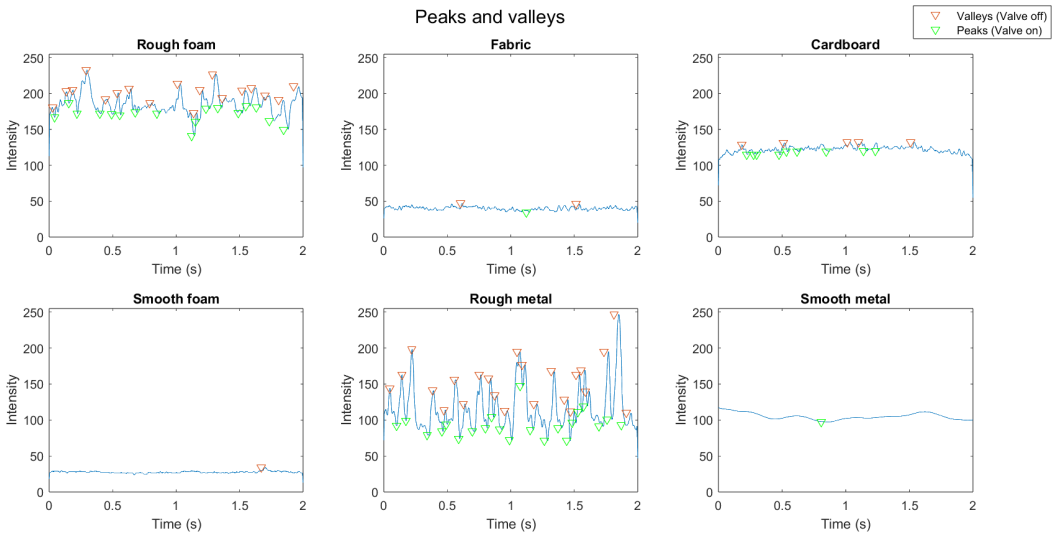

Figure B.8: Peak and valleys corresponding to the events where our pneumatic valve should be turned off and on, respectively.

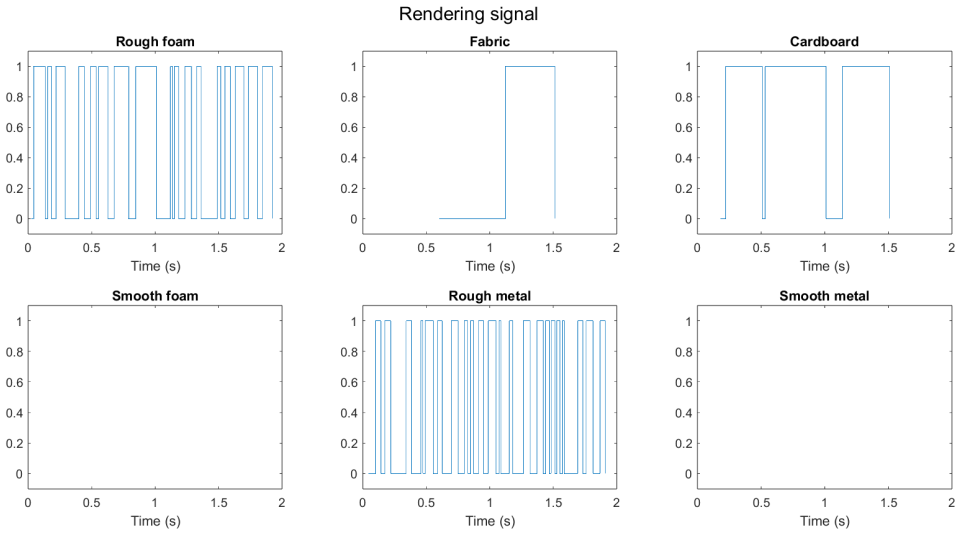

Figure B.9: Square binary rendering signals for the selected textures.

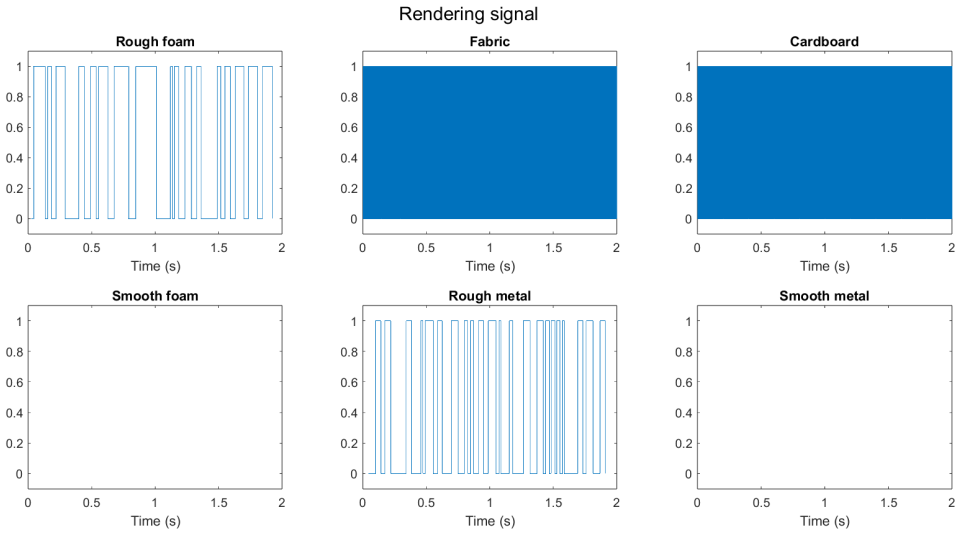

Figure B.10: Square binary rendering signals for the selected textures, where cardboard and fabric have been replaced by 300 Hz waves to account for their fine surfaces.

B.3. Compliance rendering

The figures below illustrate the process used to generate the signals simulating pressing and static contact cues. The original SENS3 dataset provides data for only ten seconds, with an emphasis on the pressing phase, while the static contact phase lasts less than five seconds. Since our simulation extends for thirty seconds, we prolonged the static contact phase to cover the majority of the simulation duration. Additionally, due to the limitations of our system, our rendering approach focuses solely on simulating the pressing and releasing forces by replicating their slopes, while the force during the static contact phase is simplified to remain constant.

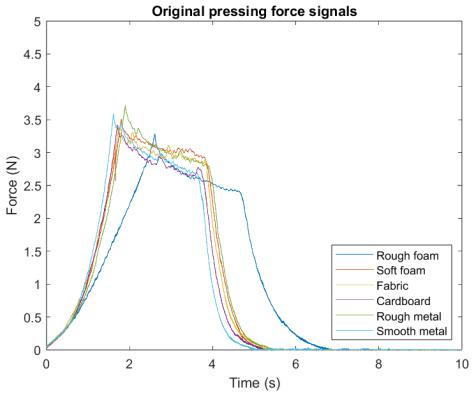

Figure B.11: Original pressing signals from the SENS3 database for the selected textures.

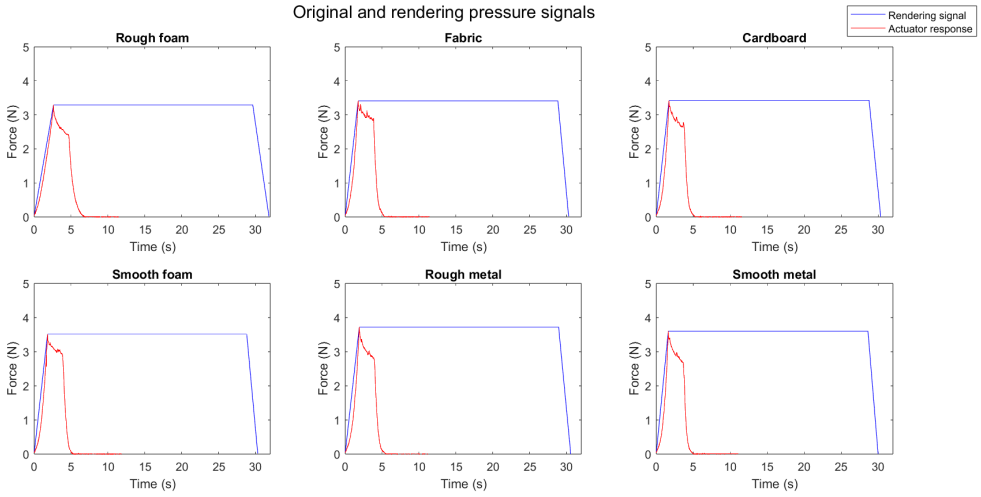

Figure B.12: Original and rendering pressing signals for the selected textures.

Texture	Pressing speed (N/s)	Lin. act. inflation speed (cm/s)	Releasing speed (N/s)	Lin. act. deflation speed (cm/s)
Rough foam	1.2618	0.8824	-1.0978	-0.8824
Fabric	1.9583	1.7510	-1.9666	-1.8152
Cardboard	2.0055	1.7928	-1.6480	-1.5708
Smooth foam	1.9499	1.7413	-1.9539	-1.8524
Rough metal	1.9620	1.7608	-1.6852	-1.6440
Smooth metal	2.2279	1.9481	-1.9624	-1.8793

Table B.2: Pressing and releasing slopes computed from the original pressing data and corresponding linear actuator speed for the selected textures.

C

Psycophysical experiment

C.1. Texture selection

The following figures below represent the results, normalized from -1 to 1, of the principal component analysis (PCA) applied to the SENS3 database adjective ratings. For roughness, values close to 1 indicate rough surfaces, while values closer to -1 indicate smoother textures. In the temperature dimension, positive values correspond to surfaces perceived as hotter, whereas negative values correspond to surfaces perceived as colder. Regarding softness, the more positive a value, the softer the texture is, while more negative values indicate a stiffer perception.

Texture	Roughness	Softness	Temperature
Rough foam	0.7542	0.3468	0.3983
Fabric	-0.2951	0.1097	0.1008
Cardboard	-0.1282	-0.0271	0.0337
Smooth foam	-0.4120	0.1160	-0.0200
Rough metal	0.4104	-0.1619	-0.1957
Smooth metal	-0.9683	-0.5053	-0.8164

Table C.1: SENS3 normalized adjective ratings in the roughness, softness and tempearture dimensions for each of the selected textures.

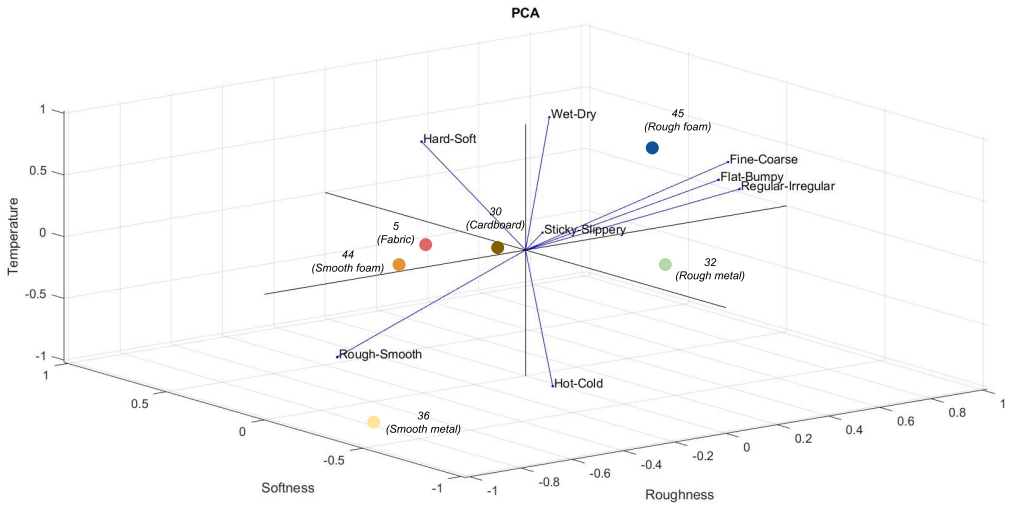

Figure C.1: Principal component analysis (PCA) three-dimensional plot showing the six selected textures.

C.2. Experimental procedure

Below, the two GUIs presented to the participant to first rate the real textures, and then perform the texture matching and virtual texture rating tasks.

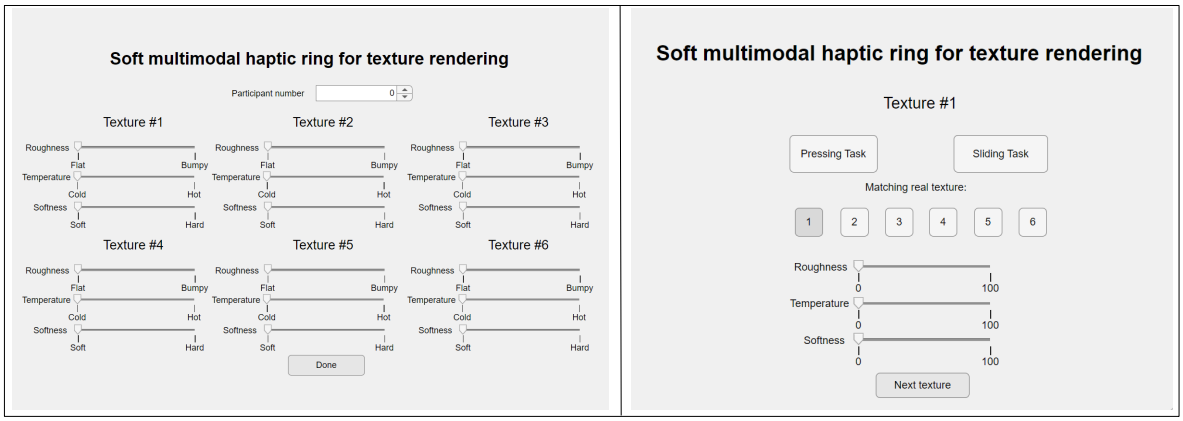

Figure C.2: Graphical user interface for real texture rating (left), and to control, rate and match the virtual textures (right).

D

Results

D.1. Texture validation

Validation of each of the selected textures in each modality is shown below by comparing the rendering signal and the actual actuator response. The thermal dimension was evaluated using the miniature thermistor embedded in the ring, while the pressure and vibration signals were measured using a custom 3D-printed setup incorporating a force sensor.

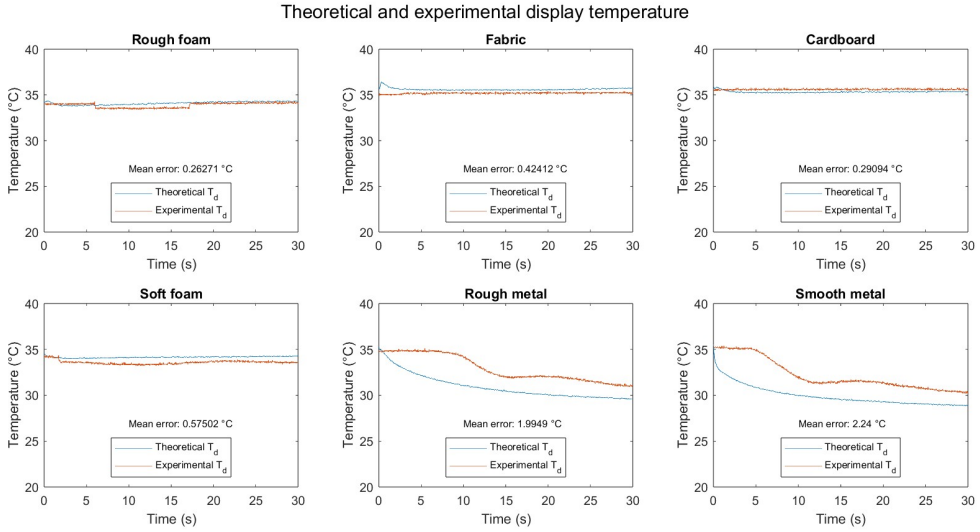

Figure D.1: Theoretical and experimental surface display temperature for the selected textures

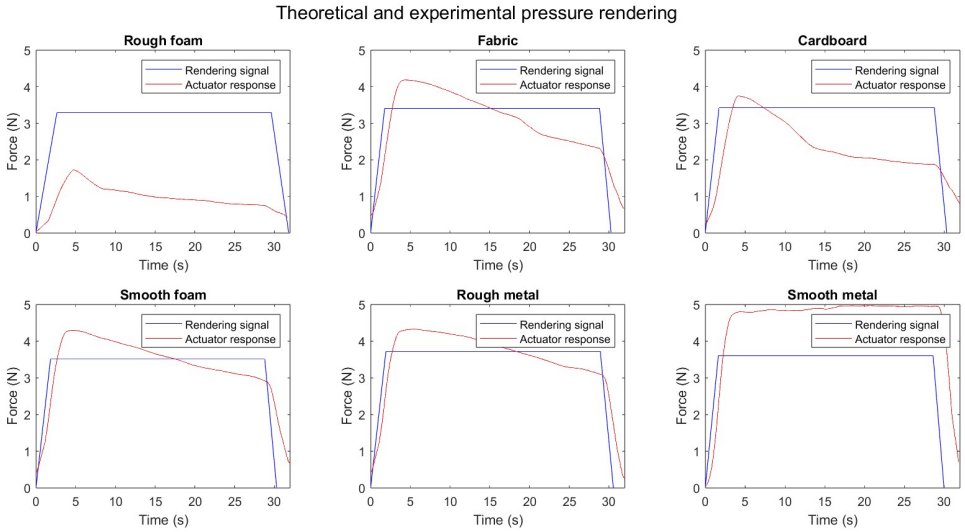

Figure D.2: Theoretical and experimental compliance rendering signals for the selected textures

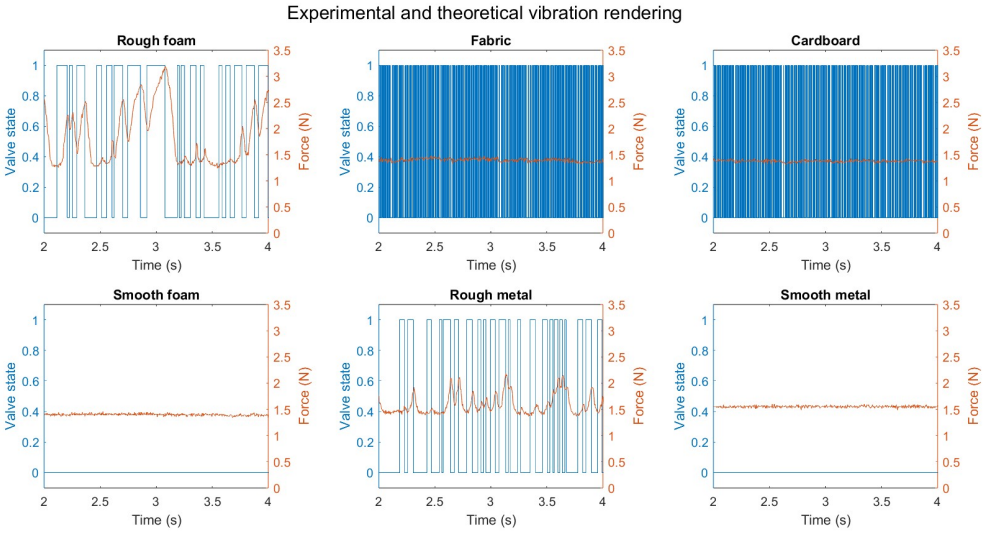

Figure D.3: Theoretical and experimental roughness rendering signals for the selected textures